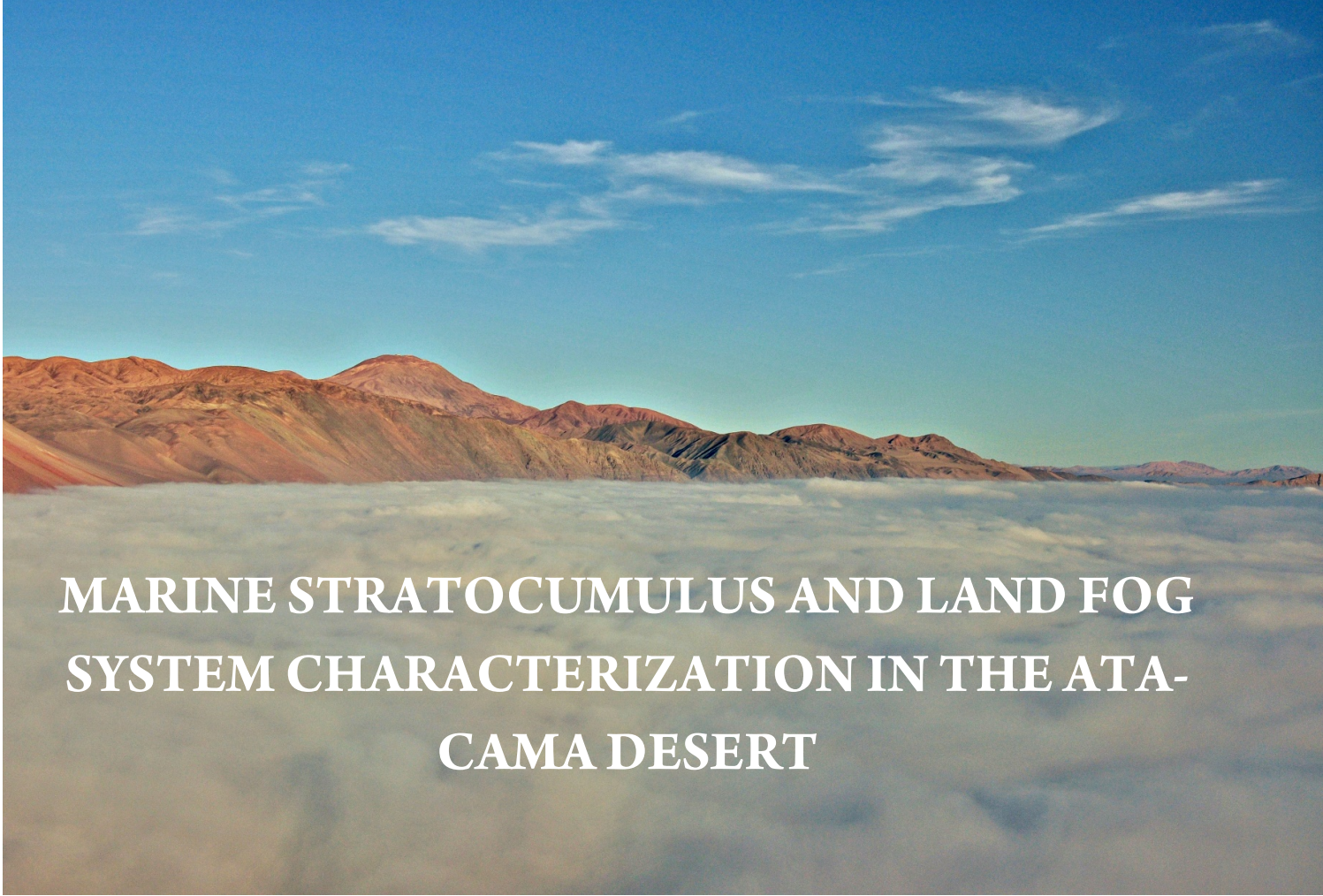




**WAGENINGEN**  
UNIVERSITY & RESEARCH



**MARINE STRATOCUMULUS AND LAND FOG  
SYSTEM CHARACTERIZATION IN THE ATA-  
CAMA DESERT**

**Felipe Lobos Roco, MSc Climate Studies**

**Supervisor: Jordi Vilà**

**ABSTRACT**

The fog in the Atacama Desert, associated with the sub-tropical marine stratocumulus cloud (Sc cloud) has been studied as an alternative freshwater resource (Schemenauer & Cereceda 1994). However, the physical processes that control the formation, maintenance and dissipation of fog, as observed over land, are not yet well understood (Cereceda et al. 2008a). This MSc research aims to characterize and quantify the Marine Sc cloud and its influence in the land fog system, by intensively using surface observations, remote sensing, and by modeling results in the Weather Research Forecasting (WRF) Model. Based on the observations located at different heights, two main regimes of fog events are identified: (a) one characterized by a thermal stratification and (b) the other by well-mixed profiles of the state variables. The latter is strongly related to periods of fog formation and maintenance. To obtain this classification we use surface observations and a simple parcel method to infer the characteristics of Sc cloud. Our findings show that cloud depth has an annual average of 622 m with a seasonal variability from 405 m in autumn to 737 m in winter. The diurnal cycle of heat fluxes from the land surface tends to decrease the cloud depth from night to afternoon and increases the cloud depth during the evening, a process that is associated with observed fog ( $>2 \text{ l m}^{-2}$ ). The cloud water content calculated by applying the parcel method is corrected and compared with fog measurements, showing that less than 30% of the liquid water is trapped by collectors. To complete the study, we use WRF to reproduce a well-mixed representative case. Model results indicate that sea surface temperature (SST) and the topography are key features in the formation and maintenance of fog.

*In memory of Felipe Herrera and Marco Vera, mentors and friends in the mountains*

This MSc Thesis describes the physical characteristics of the marine Sc cloud and its influence in the land fog system in the Atacama Desert. By using limited surface observations and modeling results, we present a first approach to: (1) the main physical characterization and quantification of the Marine Sc cloud influencing the land, (2) the quantitative relation between fog measurements and the water available in the cloud, and (3) the vertical and horizontal modelling of a representative fog event using the Weather Research Forecasting Model (WRF).

<b>1. Introduction</b>	
1.1. <i>Background</i>	6
1.2. <i>Motivation</i>	7
1.3. <i>Research questions</i>	7
<b>2. Methodology</b>	
2.1. <i>Surface observations</i>	8
2.1.1. <i>Criteria to define ABL regimes</i>	9
2.1.2. <i>Cloud base determination</i>	9
2.1.3. <i>Cloud top determination</i>	10
2.1.4. <i>Cloud depth determination</i>	10
2.1.5. <i>Physical relation between fog collection and cloud water content</i>	10
2.2. <i>Regional simulation of Sc cloud influencing the land</i>	11
2.2.1. <i>Simulation of the Sc cloud arriving the continent</i>	12
2.2.2. <i>Evaluating the importance of geographical local factors in the fog occurrence</i>	
<b>3. Physical Characterization of the marine stratocumulus cloud and its influence on the land</b>	
3.1. <i>ABL Regimes</i>	13
3.1.1. <i>Well-mixed regimes</i>	14
3.1.2. <i>Stratified regimes</i>	15
3.2. <i>Vertical characterization of the Sc cloud</i>	15
3.2.1. <i>Annual and seasonal cloud depth characterization</i>	16
3.2.2. <i>Diurnal dynamics of Sc cloud</i>	17
3.3. <i>Physical relation between fog collection and cloud water content</i>	19
3.3.1. <i>Relations between fog and cloud water content</i>	19
3.3.2. <i>Efficiency of the standard fog collector</i>	20
<b>4. Regional modeling of a representative fog event</b>	
4.1. <i>Simulation of the Sc cloud influencing the land</i>	23
4.1.1. <i>Vertical characterization</i>	23
4.1.2. <i>Spatial variability of the fog event</i>	26
4.2. <i>Importance of geographical local factors on fog dynamic</i>	27
4.2.1. <i>Influence of topography</i>	27
4.2.2. <i>Influence of sea surface temperature</i>	28
<b>5. Discussion</b>	30
<b>6. Conclusion</b>	32
<b>7. References</b>	33
<b>8. Appendix</b>	
8.1. <i>Well-mixed and stratified regimes analyze</i>	35
8.1.1. <i>Well-mixed</i>	35
8.1.2. <i>Stratified</i>	37
8.2. <i>Diurnal variability of the well-mixed days</i>	38

## 1. INTRODUCTION

The next chapter introduces the background about the fog phenomenon in the Atacama Desert related to the marine subtropical cloud formation. The importance of the processes understanding related to the phenomenon researched and its importance dealing with water scarcity are explained as well. Finally, the approach to the research is addressed through the research questions.

### 1.1. Background

The north of Chile is characterized as one of the driest places on Earth, where precipitation can reach less than 0.1 mm in a decade and temperature oscillates between 5°C to 30°C (Wesichet 1975). This place is the so-called Atacama Desert. Located at the tropical west face of South America, the extreme aridity of Atacama is driven mainly by three factors. Firstly, the subsidence produced by downward fluxes of the Hadley cell inhibit the vertical development of the clouds, therefore the clouds cannot precipitate. Secondly, the cold water upwelling by the Humboldt current reduces evaporation from the surface ocean. Thirdly, the presence of mountains higher than the marine boundary layer (MBL), blocks the humidity that is transported from the ocean to the continent. Regarding the latter, the coast of the Atacama Desert is characterized by high humidity and low thermal oscillation. This area is mainly located between 18.5° S and 23.5° S and around 70° W and is within 30 km from the coast, and frequent fog persists between 650 and 1200 m a.s.l. (meters above sea level) (Cereceda et al. 2008a).

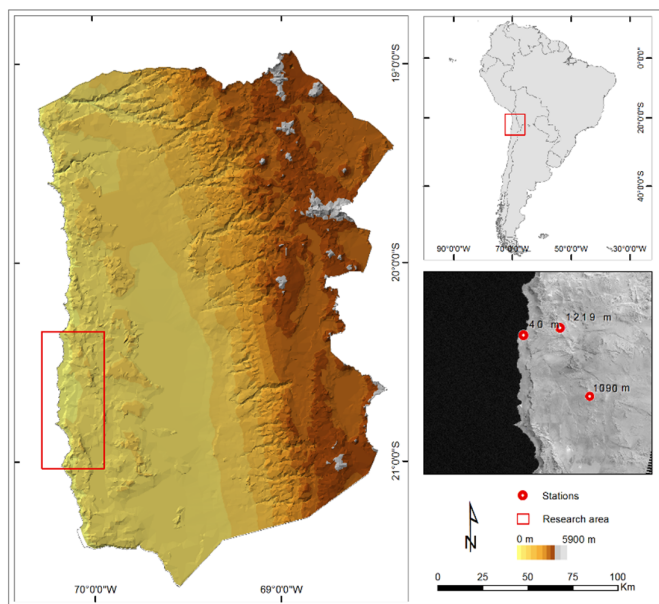


Figure 1. Research area location, stations of surface observations are placed in red dots including their altitudes.

The research area and the distribution of the surface observations used in this research are shown in Figure 1.

The fog is defined as a cloud at the surface level (Pilié et al. 1979). In the Atacama Desert, fog is closely related to synoptic phenomena as the Marine Sc cloud deck (P. Cereceda, P. Osses, H. Larrain, M. Farías, M. Lagos, R. Pinto 2002) which distributes around tropical oceans. The Sc clouds form as a result of the sea surface evaporation fluxes, which condense under high subsiding motions (Hadley cell), producing a strong capping inversion that blocks the vertical development of the clouds. Because of these processes, a large cloud deck over the southeast Pacific Ocean (SEP) is produced and transported by the winds into the continent (Bretherton & Park 2009)

For the Atacama Desert case, as Figure 2 shows the fog is produced when Sc cloud reaches the coastal mountain range (Cereceda et al. 2008a). Within a general classification of fog origin; advective, orographic and radiation fogs (P. Cereceda, P. Osses, H. Larrain, M. Farías, M. Lagos, R. Pinto 2002), the first two are formed on the Atacama coast. Advective fog is closely related with the stratocumulus cloud presence above the Pacific Ocean. These low clouds are transported by the wind from the Pacific Ocean and are trapped by coastal mountains (Klemm et al. 2012). The orographic fog is formed in situ on the windward slope facing the ocean (P. Cereceda, P. Osses, H. Larrain, M. Farías, M. Lagos, R. Pinto

2002). The typical length scales of this phenomenon reach an order of 100 km, but its arrival on land is produced on a smaller scale in the order of 10 km.

### 1.2. Motivation

Freshwater has always been the most vital natural resource for life, well-being, and development, where its uses must be shared for all parts of the biosphere (Schewe et al. n.d.). In dry regions, water is even more important because it creates tensions between civil society, environment, and industry. The Atacama Desert region is characterized by the presence of industrial activities, which are contrasted with productive agriculture zones, indigenous areas, and fragile ecosystems, where all of them are strongly dependent on fresh water (Oyarzún & Oyarzún 2011). The complex geography of the Atacama has made it difficult to diversify the water sources, these are currently extracted almost exclusively from Andes highlands water storages, causing serious damage to the environment (Aravena 1995). In that context, new water sources like the fog freshwater can play a key role by facing the water scarcity (Schemenauer & Cereceda 1994).

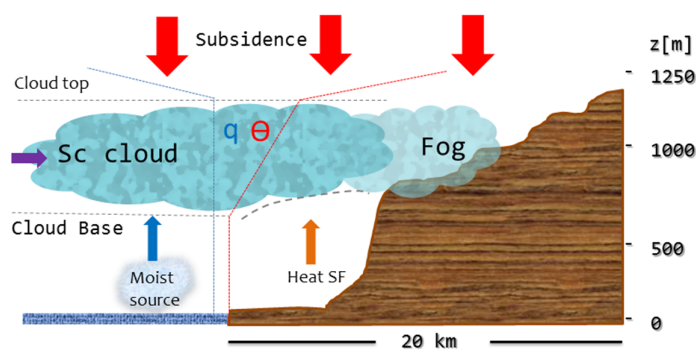


Figure 2. Physical process associated to the Marine Sc cloud formation and land fog system.

The coast of the Atacama Desert has been studied largely in terms of annual-interannual fog variability and its relation to macro-climatic phenomenon (del Río, 2016), the spatial and temporal distribution of Sc clouds (Osses et al. 2005), and relict vegetation in the so-called fog Oases (Muñoz et al. 2001). For freshwater uses, in order to study the potential of collectible water and by using standard fog collectors

(Schemenauer et al. 1994), researchers have measured annually means of fog collected around  $7 \text{ l m}^{-2}$  per day at 850 m a.s.l. and  $1.1 \text{ l m}^{-2}$  per day at 1100 m a.s.l. (Cereceda et al. 2008a). However, these studies have had to face limited quantity and quality of observations (Cereceda et al. 2008a), mainly due to the lack of meteorological stations and the low frequency of the measurements. Because this limitation, there is not yet a deep understanding of processes that control fog formation, maintenance and dissipation (Cereceda et al. 2008a), especially concerning on a physical characterization and quantification of marine Sc and its influence on the land.

Thus, considering these two reasons, the research challenge of the thesis is focused on the physical characterization of the marine Sc cloud and its influence on the land.

### 1.3. Research questions

The research addressed three main research questions, to find a physical characterization of a representative fog event.

- 1.3.1. What are the main physical characteristics of marine Sc cloud and its influence on land?
- 1.3.2. What is the physical relation between fog collected and the cloud water content?
- 1.3.3. Can the main characteristics of the fog event be modeled at the regional level?

## 2. METHODOLOGY

The following chapter describes the research strategy we follow. This was divided into two phases: The characterization obtained from surface observations and the regional modeling results. The next figure shows the general strategy.

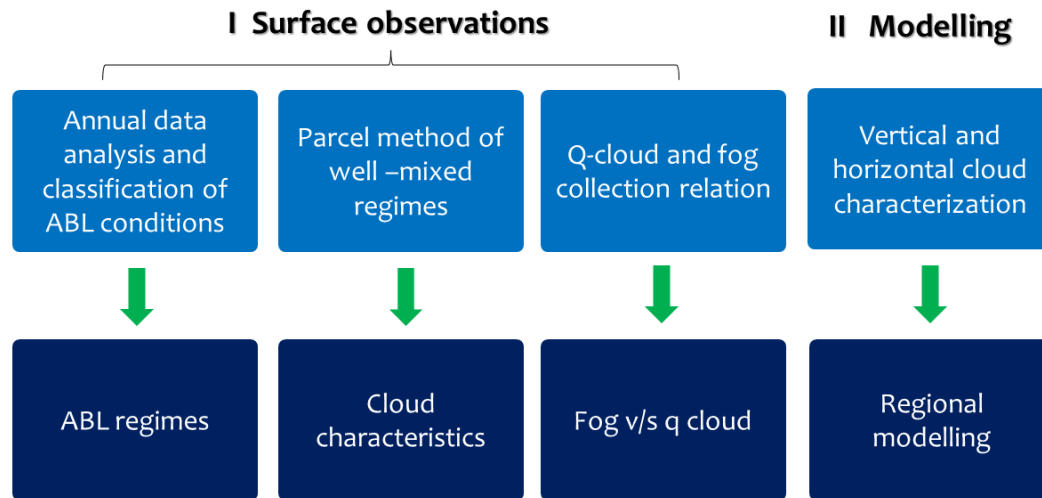
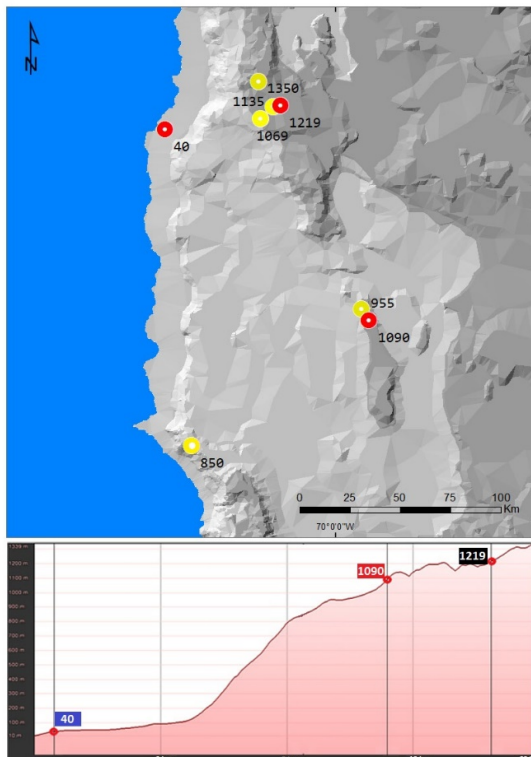


Figure 3. Research strategy followed, divided in two main faces; surfaces observations and modelling results.

### 2.1. Surface observations

The input of our research were surface observations, which were taken from meteorological stations placed on a steep slope facing the ocean at different altitudes (20.5° S – 70° W). Figure 4 shows the location of surface observations and the final selected ones in their spatial and vertical distribution.

The meteorological stations belong to two different networks; 40 m is the meteorological station of the Airport Diego Aracena of Iquique city. The rest are part of a network of a research project that studies the Tillandsia ecosystems and their relation to fog presence, supported by the Catholic University of Chile and the Heidelberg University of Germany. The stations have a frequency of measurements of every hour and they have been measured from 1998 onwards, although not all of them.



From the entire period of observations, we focus on the year 2015, because the most part of meteorological stations had been installed from that year on. Moreover, we choose stations located at different altitudes and within 20 km from the coast, because the fog is frequent in this area. Since our main aim is to relate the surface characteristics to fog formation, the selected stations require measurements of surface pressure, air temperature, relative humidity, fog collection and wind component. The final stations selected are 40 m (blue), 1090 m (red) and 1219 m (black) with an hourly frequency of measurements.

The meteorological stations belong to two different networks; 40 m is the meteorological station of the Airport Diego Aracena of Iquique city. The rest are part of a network of a research project that studies the Tillandsia ecosystems and their relation to fog presence, supported by the Catholic University of Chile and the Heidelberg University of Germany. The stations have a frequency of measurements of every hour and they have been measured from 1998 onwards, although not all of them.

Figure 4. Spatial and vertical distribution of surface observations. Upper subfigure shows the available stations (yellow) and the stations used in this work (red). Bottom sub figure shows the vertical distribution.

In the next subsection, we will describe the methods used to characterize physically the Marine Sc cloud from surface observations.

### 2.1.1. Criteria to define ABL regimes

As figure 3 shows, as a first step into the physical characterization of the Marine Sc cloud and its influence on land, we classify the atmospheric boundary layer (ABL) in two regimes: well-mixed and stratified. For that, we analyze the complete observations of 2015 and we select the days with more fog observations at the different stations with a focus on April, July, August, September, and October. In total 9 days have been selected due to data quality and their interest to distinguish different behavior between different fog characteristics.

The second step calculates conserved variables of potential temperature ( $\Theta$ ) and specific moisture ( $q$ ) for each station, using as a reference level of 40 m. In doing so, we assumed a vertical distribution of stations, 1090 m, and 1219 m, above the reference station, to know the vertical structure of chosen days. In other words, we get an advantage of the steep slope to work the data from stations as if they were placed on a meteorological tower (Like the Cabauw tower in the Netherlands).

The last step used, as the first criterion, specific moisture and as a second criterion potential temperature, to see if the ABL was classified as well-mixed or stratified. We were tolerant with the diurnal variability of the station as 1090 m and 1219 m to be placed farther from the sea (20 km).

For a well-mixed regime:

- Moisture:  $\frac{\partial q}{\partial t} (1219m - 40m) \leq 3gr\ kg^{-1}$
- Potential temperature:  $\frac{\partial \Theta}{\partial t} (1219m - 40m) \leq 2K$

For a stratified regime:

- Moisture:  $\frac{\partial q}{\partial t} (1219m - 40m) \geq 3gr\ kg^{-1}$
- Potential temperature:  $\frac{\partial \Theta}{\partial t} (1219m - 40m) \geq 2K$

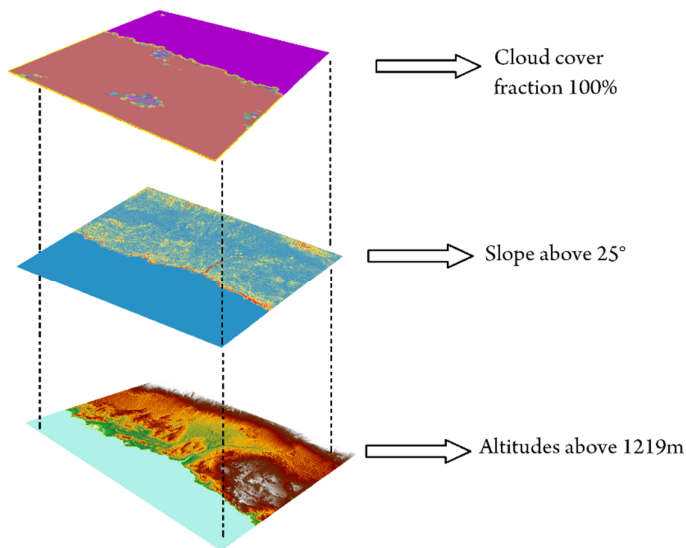
### 2.1.2. Cloud base determination

Of the total days analyzed and classified into the regimes, we selected the most common to characterize the Sc cloud vertically: the well-mixed regime.

The cloud base (CB) was characterized applying the parcel method to the well-mixed regimes. The parcel method assumes that an air parcel is lifted from the surface without entrainment during the lifting. The air parcel follows the dry and wet adiabat. For the case of our observations, we used as pressure reference the station placed at 40 m and we performed the method for 40 m, 1090 m, and 1219 m stations. The parcel method allows us to simulate virtually the vertical profile of the ABL in terms of potential temperature and specific moisture. With the projection of the potential temperature and specific moisture, we can also infer the water liquid potential temperature ( $\Theta_l$ ) and the adiabatic cloud water content ( $q_{la}$ ). These thermodynamic variables allow us to calculate the level where air condenses the lifted condensation level (LCL). As we are studying an ABL cloud we can assume that LCL is the CB.

### 2.1.3. Cloud top determination

Even though the parcel method allows us to describe the cloud vertically, it does not give us information about the cloud top (CT). For this reason, we performed a method based on remote sensing.



By using MODIS cloud cover fraction product and the Aster-GDEM digital elevation model, we calculate the mean elevation where the cloud cover fraction of 100% (representing the Sc deck) comes into contact with a steep slope ( $>25^\circ$ ) and altitudes higher than 1219 m. The first criterion is used because, under flatter slopes, the cloud can overlap lower lands and the second criteria because at 1219 m we have the highest fog observations. Figure 5 shows the procedure followed.

Figure 5. Diagram followed to estimate the Cloud Top by using remote sensing procedure.

### 2.1.4. Cloud depth determination

Once determined, the CB and CT were subtracted to obtain the cloud layer or cloud depth (CD) as a function of local time. By intersecting the CD and q<sub>la</sub> obtained from the parcel method, we can quantify the adiabatic cloud water content present in the cloud layer. More details about q<sub>la</sub> will be explained in the next subsection.

### 2.1.5. Physical relation between fog collection and cloud water content

To end the method of the results obtained from the maximization of the surface observations, we explain the procedure followed to obtain the physical relation between fog collection observations and cloud water content.

As was described in the cloud base determination section, the parcel method lifts an air parcel through the dry adiabat till it condenses, then the air parcel follows the wet adiabat. From this process, we determined the adiabatic cloud water content (q<sub>la</sub>) as the difference between an assumed constant specific humidity and the saturated specific humidity ( $q_t = q_{sat} + q_{la}$ ). Vertically, the bottom and top of q<sub>l</sub> are determined by the CB and CT respectively. Once we estimated the adiabatic q<sub>l</sub> (q<sub>l</sub> obtained from the parcel method) we applied a correction factor in order to have more realistic values. The correction factor was determined as a linear function between the maximum values of q<sub>la</sub> and q<sub>l</sub> obtained in campaign observations (Duynerke et al. 1995, Garreaud & Munoz 2004). The linearity of the correction factor is supported by field observations (Duynerke et al. 1995, Stevens et al. 2003), where q<sub>l</sub> increases from the CB linearly till sub-layer of the CT. This correction factor changes with height and represents a 20% of the q<sub>la</sub>. The following equation explains the development of the correction factor.

$$(1) \quad q_{lc} = q_{la} \times 0.2$$

Where  $q_{la}$  is the adiabatic  $q_l$  obtained from the parcel method,  $q_{lc}$  is the corrected  $q_l$  and 0.2 is the correction factor.

Once we corrected the values of  $q_l$ , we performed a homogenization between the units of fog collection measurements ( $l\ m^{-2}$ ) and the units of  $q_{lc}$  ( $kg_w\ kg_a^{-1}$ ). Both units were transformed to  $kg\ m^{-3}$  as the following equations show.

$$(2) \text{ fog collection } \left( \frac{l}{m^2} \right) = \frac{l}{m^2} \times \frac{1}{m/s} \times \frac{1}{3600\ s} \times \frac{kg}{l} = \frac{kg_w}{m^3}$$

$$(3) \text{ } q_l \left( \frac{kg_w}{kg_a} \right) = \frac{kg_w}{kg_a} \times \frac{kg_a}{m^3} = \frac{kg_w}{m^3}$$

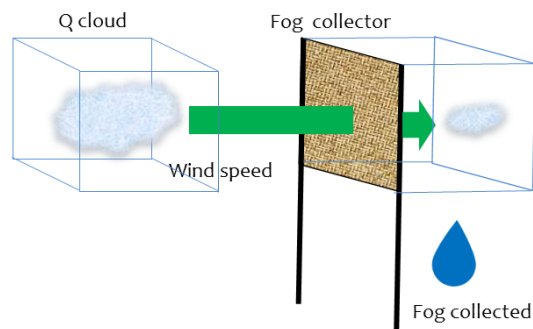


Figure 6. Diagram of the method used to compare fog collection with cloud water content ( $q_l$ )

In equation (2), the units of fog collections were divided by the wind speed in order to transform the area of the mesh into a volume ( $m^2$  to  $m^3$ ), then assuming the observations are an average of one hour, we divided by the time in seconds. Finally, we transform the liters into kilograms obtained as a result  $kg_w\ m^{-3}$ .

In equation (3), we use the density of the air ( $kg_a\ m^{-3}$ ) to transform the units of  $q_l$  into  $kg_w\ m^{-3}$ . Even though the physical meaning of this scaling factor is not fully clear yet, the next figure explains the idea in a simple way.

## 2.2. Regional simulation of Sc cloud influencing the land

The second phase in the methodology was the simulation by using WRF, of the cloud characteristics obtained from surface observations. Firstly, we simulate the marine Sc cloud, focusing on its influence on the continent, this experiment was set as a control run. Secondly, we explore the influence of geographical local factors through two sub-experiments: absence of topography and changes in sea surface temperature (SST).

### 2.2.1. Simulation of the Sc cloud arriving the continent

The numerical setup performed in WRF for the control case is described below.

- **Integration time:** 20-22, July 2015. The 20<sup>th</sup> is used as spin-up day.
- **Day analyzed:** 21-07-2015
- **Horizontal resolution:**

Domain	D01	D02	D03	D04
Size grid cell	31 x 31	49 x 49	49 x 49	50 x 60
Resolution	4 km	2 km	2 km	1 km

- **Vertical Resolution:** 29 Eta levels, with 20 in the first 2000 m.
- **Initial boundary layer conditions:** ECMWF for -21, -70 (lat/long) every 6 hours.

For this experiment, we set default parameterizations of which the main components are described as follow:

<b>Physics</b>	<b>Scheme used</b>
Microphysics	WSM 3-class simple ice scheme
Surface layer	Revised MM5 Monin-Obukhov scheme
Land surface	Unified Noah land-surface model
<b>Boundary layer</b>	<b>UW boundary layer scheme from CAM5</b>
<b>Convection</b>	<b>Modified Tiedtke scheme (ARW only)</b>
Optical cloud	Cloud effect to the optical depth in radiation

Regarding the parameterization schemes in bold, we selected for boundary layer the scheme **UW**. This is a first-order closure scheme, which uses moist conserved variables and explicit entrainment closure for convective layers (Bretherton & Park 2009). According to the authors, this scheme has a physically realistic parameterization for marine Sc-topped boundary layer. For the convection scheme, we selected the **Modified Tiedtke** scheme (Zhang et al. 2011). This scheme uses a convective available potential energy closure and includes the organized entrainment and detrainment based on a cloud plume model (Nordeng, 1995, cited from Zhang et al. 2011). The advantage is that amongst other schemes this is more active in parameterizing shallow convection, where it plays a fundamental role in the inversion base and the low clouds (Zhang et al. 2011). Finally, we must mention that the observations of SST provided by the NOAA, set the SST 1.5K higher than in the initial boundary layer conditions, so we increase the SST in the simulation to have a more realistic representation.

#### 2.2.2. Evaluating the importance of geographical local factors in the fog occurrence.

The second experiment uses the last experiment as a control case in order to compare the Sc-simulation under three different conditions:

- Flat topography: here we set a flat topography for all domains for altitudes higher than 40 m (the reference station). This simulation is made to understand how Sc cloud deck performs without the topography barrier.
- Warm Ocean: we increase the SST in 3 K. This amount of increase was set based on the El Nino year 1998, where SST in the research area was 2 K higher than 2015 (NOAA). This run aims to simulate an extreme situation of high SST and its influence on cloud formation.
- Cold Ocean: we perform the same procedure than Warm Ocean, but decreasing the SST by 3 K.

### 3. PHYSICAL CHARACTERIZATION OF THE MARINE STRATOCUMULUS CLOUD AND ITS INFLUENCE ON THE LAND

This chapter describes the characteristics of the observed convective boundary layer based on surface measurements. The observations are classified according to the stability criteria described in the previous section. The vertical structure of the representative foggy days in terms of cloud base, cloud top, cloud depth, and cloud water content is explained as well. Finally, the physical relation between fog collected and cloud water content is shown. This chapter aims to answer the first two research questions.

#### 3.1. ABL Regimes

The year 2015 presents two kinds of regimes: (1) regimes characterized by a well-mixed layer condition and (2) regimes characterized by a stratified layer condition. Different vertical structures characterize these regimes in terms of potential temperature, moisture, fog collection, diurnal variability and cloud depth (Table 1).

Table 1. Summary of the results of the ABL and Sc cloud characterization for well-mixed (Wm) and stratified (St) regimes. The regimes are described by the dates of the observations (Day); the Season Autumn (A), winter (W) and Summer (S); the averages of the daily difference in potential temperature between the highest and the lowest stations ( $\Delta\Theta$  [K]); the  $\Delta\Theta$  [K] filtering out the diurnal variation ( $\Delta\Theta$  [K] no diurnal); wind direction at station 40m; the averages of the daily difference in specific moisture between the highest and the lowest stations ( $\Delta q$  [g kg<sup>-1</sup>]); total fog collection per day ( $fog_{\tau}$ ); hours of diurnal variability; cloud base and cloud top.

Day	Stability	Season	$\Delta\Theta_{1219-40}$ [K]	$\Delta\Theta$ [K] no diurnal	$U_{40}$ [°]	$\Delta q_{40-1219}$ [gr kg <sup>-1</sup> ]	$fog_{\tau}$ [l day <sup>-1</sup> ]	Diurnal variability [h]	$C_{fog\ base}$ [m]	$C_{fog\ top}$ [m]
18-04-2015	Wm	A	4.07	2.38	211	0.21	7.3	9.5	886.3	1285
29-04-2015	Wm	A	6.21	3.65	166	0.54	1.1	12	860.5	1273
21-07-2015	Wm	W	2.78	2.17	249	0.52	13.52	6	784.1	1445
08-08-2015	Wm	W	2.84	2.21	199	1.15	4.05	7	651.5	1466
17-09-2015	Wm	W	3.79	1.98	202	0.91	7.12	10	667.9	1366
08-10-2015	Wm	S	3.8	2.57	202	0.93	6.63	10	593.7	1344
27-07-2015	St	W	14.21	12.9	180	4.07	5.67	20	--	--
28-07-2015	St	W	11.48	7.3	212	3.32	7.42	14	--	--
20-10-2015	St	S	12.75	11.16	188	1.95	--	20	--	--

Results shown in Table 1 show that well-mixed regimes differ from stratified regimes by presenting lower differences in potential temperature (for both daily averages and no diurnal averages), lower differences in specific moisture ( $\Delta q$ ), higher fog collection and lower diurnal variability time (Table 1). Additionally, the wind direction is also shown to characterize the Sc cloud approximation to the land, coincidentally with literature (Cereceda et al. 2008a), the predominant winds come from S and SW (180 - 225°). Finally and linking with the next section of the results, we present the daily average of cloud base and cloud top for the well-mixed regimes.

The well-mixed fog days present a characteristic seasonal variability, where winter days show generally lower values than summer and autumn for most variables. This difference, however, is lower than 5 K in term of  $\Delta\Theta$ , evidencing a strong marine control on boundary layer dynamics. The diurnal variability is also lower in winter than in spring and autumn at higher stations (< 7 hours per day) (Table 1). Specific moisture is higher in the autumn day around 10 g kg<sup>-1</sup> and lower in winter and spring. Fog collection also shows a slight seasonal variation, reaching the highest values in winter and the lowest in autumn (Table 1).

To describe the diurnal evolution of fog, potential temperature, and moisture, we focus on one well-mixed and one stratified day. Figure 7 shows observations at 21-07-2015 (a) and 28-07-2015 (b), corresponding to a representative well-mixed and stratified fog regime. The other observations can be found in Appendix 8.1

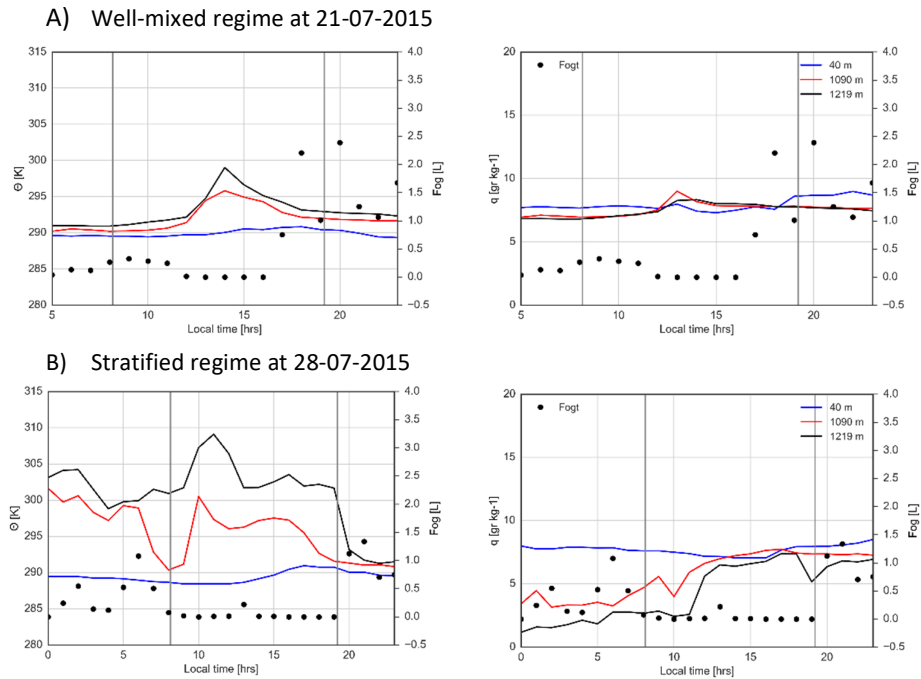


Figure 7. Total fog collection (black dots), potential temperature (left) and specific moisture (right) as a function of local time. Values represented for stations placed at 40 m, 1090 m, and 1219 m, during well-mixed (a) and stratified (b) regimes. Sunset and sunrise have been set by grey lines.

### 3.1.1. Well-mixed regimes

We find that fog is mainly produced and collected during the afternoon, evening and night hours with peaks above  $2 \text{ l m}^{-2}$  (Table 1). Although daily amounts of fog collected are variable, they coincide with historical observations of around  $7 \text{ l m}^{-2} \text{ day}^{-1}$  (P. Cereceda, P. Osses, H. Larrain, M. Farías, M. Lagos, R. Pinto 2002). It is remarkable that fog is collected when ABL is well-mixed in terms of potential temperature and specific moisture, for example at 10:00 and 20:00 local time, where diurnal variability is not present (Figure 7 a).

The potential temperature shows a flat and stable distribution during the day, varying between 290 K and 300 K (Figure 7 a). All stations showed potential temperatures in the range of 2 - 4 K across different altitudes, evidencing a well-mixed layer condition. A diurnal variability can be seen in the higher levels (1090 m and 1219 m) between 12:00 and 17:00 local time (Figure 7a), probably because higher stations are located farther from the ocean (Figure 4). From the potential temperature shown in Figure 7a, we can characterize the stations, and therefore the research area, as located in a transition zone between the marine boundary layer (MBL) and the continental boundary layer (CBL). Here the lowest and closer-to-the-sea station has no diurnal evolution (40 m) and the higher and farther inland stations have it.

Finally, specific moisture shows a very stable diurnal evolution, where moisture distributes equally in all levels (40 m, 1090 m, and 1219 m) in ranges from 7 to  $10 \text{ g kg}^{-1}$  (Table 1). The diurnal variability is slightly noticeable during the afternoon around 13:00 local time and it disappears during the evening (from 18:00). According to our classification criteria (Methodology, Section: 2.1.1), this specific moisture condition is the most important in characterizing a well-mixed layer condition.

### 3.1.2. Stratified regimes

Contrary to the typical well-mixed fog regimes, the stratified regimes present larger variations in potential temperature and moisture (Figure 7 b), which change drastically from the lower to the higher levels. In terms of fog collection, we observed a similar dynamic distribution as the well-mixed days, with similar total amounts (Table 1) but with lower peaks (maximum of  $1.3 \text{ l m}^{-2}$ ). It is noticeable that at later hours of the day (from 20:00 local time; Figure 7a) the fog collection observed coincides with well-mixed profiles of the potential temperature and specific moisture (curves closer to each other). This pattern confirms that fog can be collected mainly under well-mixed layer regimes.

The potential temperature shows a thermal stratification where lower stations have lower values than the higher stations. It is remarkable the influence of MBL in the station at 40 m, which presents a sort of steady-state behavior. Such behavior is because 40 m station is situated closer to the ocean and at lower altitudes, where marine influence can be higher. On the other hand, stations situated farther from the ocean and at higher altitudes show diurnal variability in potential temperature, where differences between the lowest and highest stations can reach around 14 K (see  $\Delta\theta$  in Table 1), evidencing a transition towards the CBL.

Moisture profiles start with higher values ( $9 \text{ g kg}^{-1}$ ) at the lower stations and decrease with altitude ( $1 \text{ g kg}^{-1}$ ). This day presents a small evolution from a stable layer towards a well-mixed layer, from 12:00 local time, where fog observations are placed.

The fog is observed in both regimes, with no significant differences between them. However, the fog collection seems to be more associated with the well-mixed regime than the stratified one. This is because the arrival of the Marine Sc cloud is also formed under well-mixed conditions. For the entire analyzed year, well-mixed regimes were much more frequent than stratified regimes. For this reason, we selected the well-mixed regimes to characterize vertically the Sc cloud and its influence on the land.

### 3.2. Vertical characterization of the Sc cloud.

As shown in the previous section, fog observations seem to be more related with well-mixed regimes than stratified regimes. In this section, we show results on the vertical cloud characterization under well-mixed regimes.

In the methodology, we applied the parcel method to describe thermodynamically the vertical structure of the ABL under well-mixed conditions. In order to validate this method and the comparisons between water liquid content and fog observations, here we compare and test the similarity of the following two vertical structures. First, a vertical profile applying the parcel method (40 m as reference) and second a vertical profile resulting from observations of the stations placed at the slope at different heights (black dots, Figure 8).

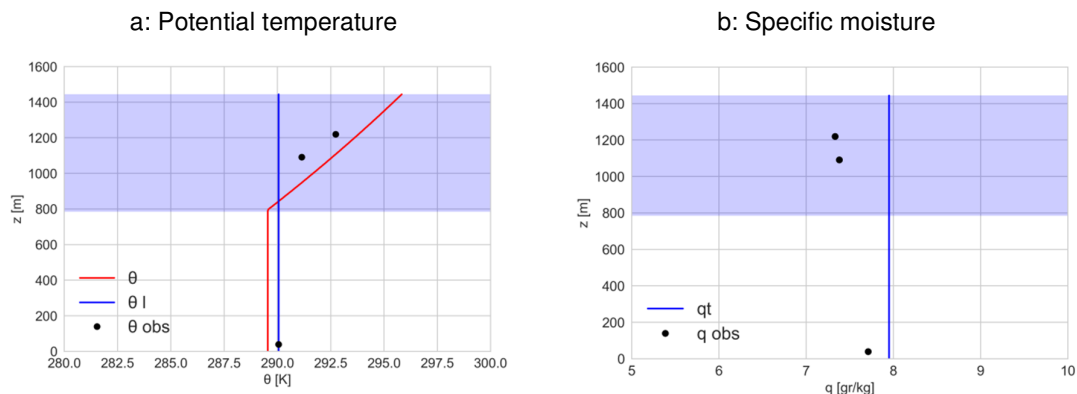


Figure 8. Comparison between the parcel method (lines) using as reference station 40 m and observations (dots) from stations located at different heights. Observations collected on 21-07-2015.

The vertical profiles resulting from the parcel method in terms of potential temperature ( $\Theta$ ), liquid potential temperature ( $\Theta_l$ ) and specific humidity ( $q_t$ ), do not differ significantly from the profiles resulting from observations (Figure 8). The Chi-square test showed no significant differences between observations and the parcel method ( $p$ -value=0.9).

Given that the parcel method has proven to be a valid methodology to infer the cloud characteristics so far, here we present the results of this method for well-mixed regimes. The characterization of the Sc cloud is described using the following features: cloud base (CB) assumed as the lifted condensation level (LCL), cloud top (CT) assumed as the boundary layer height, and cloud depth (CD) understood as the difference between CT and CB.

### 3.2.1. Annual and seasonal cloud depth characterization

Figure 9 a shows CD annual mean and variability as a function of local time. The annual means of CB, CT, and CD are 740 m, 1369 m, and 622 m, respectively. CB presents an annual variability of 150 m around the mean, which corresponds to the standard deviation of the LCL from all well-mixed days analyzed. This means that CB varies yearly from 590 m to 890 m. CT varies less than CB, presenting a variability of only 73 m over the year. From Figure 9 we also observe a diurnal variability present in all analyzed days, affecting annual CD during the daytime. This is noticeable from 10:00 to 21:00 local time, where we find a thinning from the morning (10:00) to the afternoon (16:00) and a thickening from afternoon to evening (21:00).

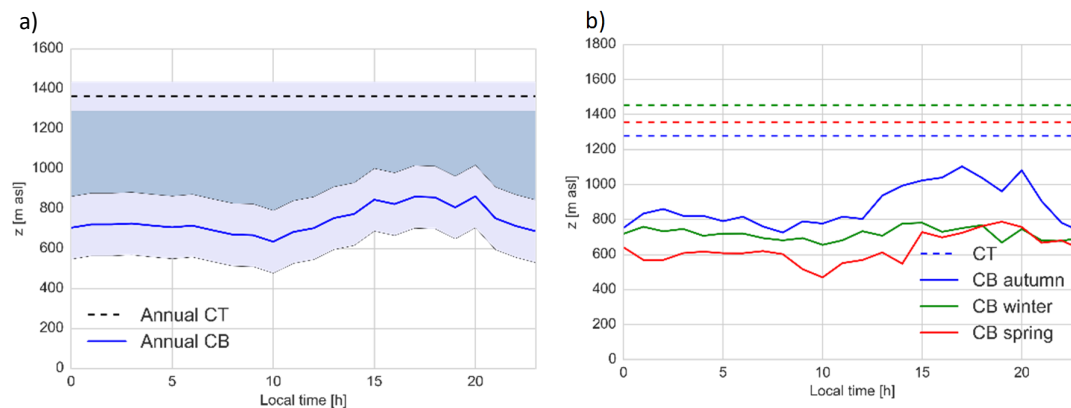


Figure 9. (a) Annual mean of cloud depth and (b) seasonal mean cloud depth, as a function of local time, represented as the cloud top and cloud base, calculated from the reference station (40 m) for 2015.

The cloud characterization presented here agrees partly with observational field campaigns and modeling reported in the literature (Stevens et al. 2003, Garreaud & Munoz 2004, Duynkerke et al. 1995, Cereceda et al. 2008b). Observations of marine Sc cloud done in the subtropical northeast Atlantic, however, show a thinner (CD: 320 m) and lower (CB: 380 m) Sc cloud than Sc cloud of our results (Duynkerke et al. 1995). Likewise, flight measurements on Sc cloud did in the subtropical northeast Pacific show a CD of 400 m and CB of 450 m (Stevens et al. 2003). However, we have to consider that 2015 was reported as an El Niño year, where sea surface temperature increases (Judah Cohen et al. 2017). As we explain in chapter 4, Sc cloud formation is very sensitive to the SST changes. On the other hand, other studies reported show a better agreement with our results. For example, the modeling did in the southeast Pacific region (close to our research area) shows marine Sc cloud 500 m thicker, with CB from 500 m (Garreaud & Munoz 2004). Moreover, simulations in global climate models (CAM 3.5 and GFDL) show similar CD with a high CB at 80-70°W (Wyant et al. 2010). Finally, fog observations

used for this work and also reported in the literature can help characterize the real cloud thickness and the fog, which were observed from 850 m a.s.l. to 1219 m a.s.l. (Cereceda et al. 2008b). The latter will be analyzed and discussed in the next section.

The variability in cloud characteristics described above can be explained by some physical processes. First, the diurnal variability is related with the surface fluxes that increase at daytime pushing up the CB. This explains the differences in the level where CB is calculated, where sensible heat surface fluxes are higher over land than at the sea. Also, the shortwave radiation (SW) at TC produces turbulent motions that entrain warmer and dryer air, producing a thinning of the cloud layer (Duynkerke et al. 1995). These patterns cannot be identified from our observational data, but we show it through the modeling approach (Chapter 4, regional modeling). The same process is associated with higher variability of the CB ( $\pm 157$  m), where over different seasons, the intensity of surface heat fluxes changes producing changes in the CB. In other words, the heat surface fluxes in winter are much lower than in summer, producing larger differences in the CB. Secondly, the subsidence is the second process associated with the small variability of the CT ( $\pm 73$  m). The Pacific Anticyclone is located over the research area during the summer and moves a bit NW during winter. However, it is mainly over the research area, so smaller changes in seasonal subsidence promote smaller changes in TC. Finally, from the annual mean of CD, we can state that the presence of the Sc cloud over the reference station is very stable during the year and under well-mixed regimes, presenting low variability.

As shown earlier, the seasons also affect the CD leading to variations in both CT and CB. Figure 9 b shows the seasonal CD for autumn (405 m), winter (737 m) and spring (724 m) over the year 2015. While the CD increases from autumn to spring, the CB decreases.

These changes in CB can be explained by the outgoing radiation and the moisture sources. The radiation decreases from autumn to winter decreasing the surface heat fluxes and consequently the level at which air parcel condenses (LCL). The moisture sources increase from autumn to spring allowing the condensation of air parcels at lower levels. The moisture source is closely related with the marine boundary layer, which seems to dominate during the winter. The CT reaches its highest level during winter (1445 m) when it also presents the thickest cloud layer. The latter relates to the synoptic conditions that characterize the winter, where the high-pressure present over the research area moves NW, decreasing the subsidence and allowing the ABL to grows. Finally, CD shows diurnal variability during autumn and spring daytimes, but it is stable during the whole day in the winter days.

### 3.2.2. Diurnal dynamics of Sc cloud

To complete the analysis of CD, we present the diurnal variability of a representative well-mixed day (21-07-2015) in order to analyze the relationship between CD and the fog collection observations. The rest of the weel-mixed days can be found in Appendix 8.2. Three CB values have been calculated from stations located at altitudes of 40 m, 1090 m, and 1219 m. We used the pressure measured at 40 m as a reference. Figure 10 shows the diurnal variability of cloud characteristics at date 21-07-2015 as a function of local time, as well as three schemes simulating the Sc cloud depth location and surface observations at different hours.

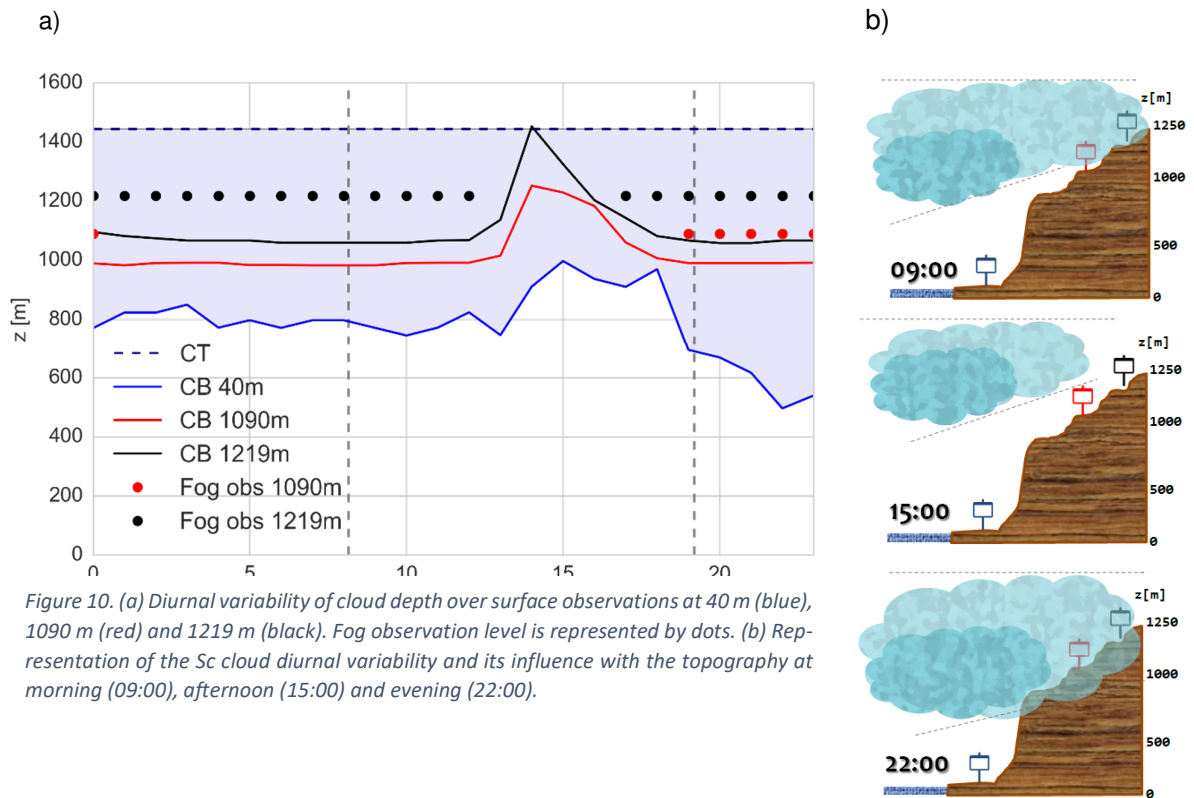


Figure 10. (a) Diurnal variability of cloud depth over surface observations at 40 m (blue), 1090 m (red) and 1219 m (black). Fog observation level is represented by dots. (b) Representation of the Sc cloud diurnal variability and its influence with the topography at morning (09:00), afternoon (15:00) and evening (22:00).

We find that CD is always thicker closer to the sea than over the land. Two processes could explain this. The first one is a thinning from the ocean to the land, as the CD is thicker closer to the sea (at the 40 m station), and becomes thinner as it moves up inland (at stations 1090 m and 1219 m). The second process is the uplifting motion of the cloud when it arrives at the mountains, as topography forces the cloud to rise. Unfortunately, our CT estimations do not allow us to confirm which process is ruling this pattern, but in Chapter 4 we discuss it using the modeling approach.

Figure 10 shows that the altitude where fog collection has been observed coincides with the cloud layer measurements. The latter is understood as a validation of the CD calculations because the fog observations are placed inside the cloud layer estimated by surface observations. During the night and morning (till 10:00 local time), the Sc cloud seems to be stable in terms of CD and only producing fog at the highest level (1219 m). The first scheme to the right represents the Sc cloud influencing the land at 09:00 local time when fog is observed at 1219 m (Figure 10). During midday (12:00 to 18:00 local time) the CD decreases above the 40 m and 1090 m stations, and at the 1210 m station, the CB reaches the CT, resulting in no clouds to be formed there. This also coincides with no fog measured at 15:00 (Figure 10 b; a scheme to the right). At 22:00 the cloud layer grows and fog is observed at 1090 m and at 1219 m station (Figure 10 b; a scheme to the right).

In summary, the diurnal dynamics of the marine Sc cloud in the research area is produced by a complex interaction between clouds and the topography. The upward and downward fluxes lead these dynamics resulting in changes in the CD, water liquid content and consequently in fog collection.

### 3.3. Physical relation between fog collection and cloud water content

To complete the analysis of physical characteristics of the marine Sc cloud and its influence on land, in this section we describe the physical relation between the amount of water collected by the standard fog collector (Figure 5) and the available water in the air ( $q_l$ ). Here, we present and discuss an approach to connect the cloud characteristics retrieved from the parcel method with the fog estimations and the results obtained from the Weather and Research Forecasting Model (WRF). Special emphasis is placed on discussing the implications of the assumptions.

#### 3.3.1. Relations between fog and cloud water content

The cloud water content ( $q_l$ ) is the amount of liquid water in the cloud and can be used to determine the relation between the marine Sc cloud and the fog at land. According to previous observational studies on Marine Sc characterized by similar synoptic conditions, i.e. high pressure on the Hadley cell branch ( $30^\circ$  N), the difference between adiabatic and observed  $q_l$  increases with height (Duynderke et al. 1995). In the large-eddy simulation of shallow cumulus, it was found that calculated values and inferred values of  $q_l$  differ around 30% (Siebesma et al. 2003). In that context, we compared the values of  $q_l$  inferred from the parcel method ( $q_{la}$ ) and adjusted it to typical values of Marine Sc.

The  $q_{la}$  calculated from the parcel method overestimates the observations in campaigns and modeling results reported in the literature. This overestimation is one order of magnitude higher, probably because the  $q_{la}$  does not consider the dilution of the parcel containing environmental air with drier and warmer characteristics (Duynderke et al. 1995). The ASTEX measurement campaign done in the NE subtropical Atlantic and the DYCOMS II field study performed in the NE subtropical Pacific, report values of Sc cloud  $q_l$  in the range of 0 - 0.5  $\text{g kg}^{-1}$  (Duynderke et al. 1995, Stevens et al. 2003). Moreover, Garreaud and Munoz (2004) performing a large eddy simulation of the marine Sc deck at Southeast Pacific (SEP), reported values in the range of 0 - 0.3  $\text{g kg}^{-1}$ . Finally, Siebesma et al (2003) showed that in the case of shallow cumulus, the  $q_l$  cloud and core observed represents between of 25% and 40% of their adiabatic value. Based on these experimental and calculated results, and in order to take into account the parcel dilution effects with the environment, we applied a correction factor to adjust our retrieved  $q_{la}$  values. Based on field campaigns the correction factor applied ( $q_{lc}$ ) corresponds to 20% of the inferred  $q_{la}$ . We realize that this 20% is a had doc value, but it is a first-order approximation.

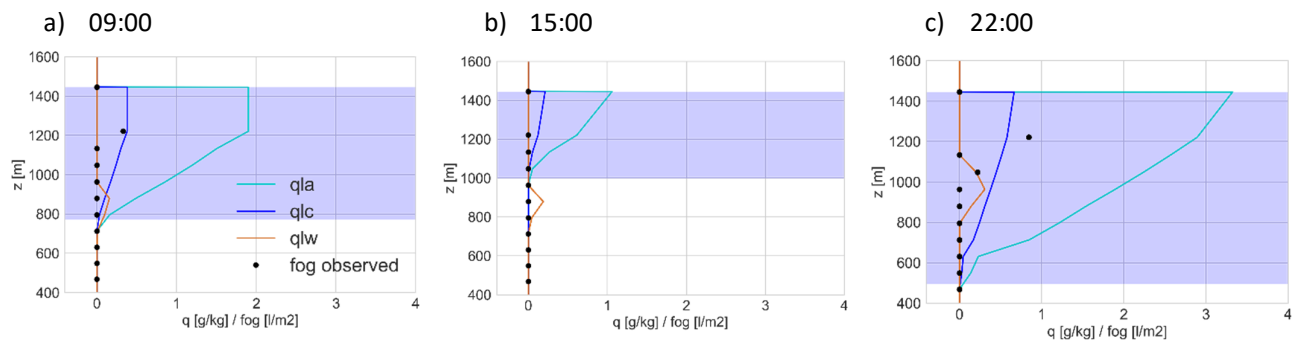


Figure 11. Vertical profiles of  $q_l$  estimated with the parcel method ( $q_{la}$ ) (reference 40m station), estimation of  $q_l$  corrected ( $q_{lc}$ ),  $q_l$  modeled by WRF ( $q_{lw}$ ) and fog collection observations at 1090 m and 1219 m as a function of height. The background represents the background represents the cloud layer inferred by surface observations. For the analyzed day 21-07-2015. Note that the fog observations is presented with different units.

Figure 11 shows the vertical profiles of  $q_l$  inferred through the parcel method, the  $q_l$  corrected, the  $q_l$  modeled in WRF and the fog observed during the morning, afternoon and night. We have found that the difference between  $q_{la}$  and  $q_{lc}$  increases with height (Figure 11), agreeing with the literature (Duynderke et al. 1995). The values of  $q_{lw}$  underestimate the inferred values of  $q_{lc}$ , but they reach the same range around 0.5  $\text{g kg}^{-1}$ .

Fog observations increase with height at the same rate as the  $q_{lc}$ , even though the units are different. Moreover, the CD play a role in the fog collection, because it seems to affect it, i.e. CD plays an important role in fog collection. Observational and modeled data suggest that fog is only formed when CD is thicker than 600 m and  $q_{lc}$  are higher than  $0.3 \text{ g kg}^{-1}$  (Figure 11 a, c). Also, the fog is observed above values of  $q_{lc}$  higher than  $0.3 \text{ g kg}^{-1}$ . The cloud water content corrected ( $q_{lc}$ ) matches with fog observations as it distributes in an altitude between 1090 m and 1219 m (09:00).

However, fog measurements were not observed at the altitude where WRF simulated the highest cloud water content (900 m). Analyzing the cloud water content modeled by WRF ( $q_{lw}$ ), we find three main aspects: (1) the values of cloud water content are close to the observations reported in other studies (Duynderke et al. 1995), and to the  $q_{lc}$  values ( $0 - 0.5 \text{ g kg}^{-1}$ ); (2) the cloud base (CB) is only well reproduced during the morning (9:00) and is underestimated at 15:00 and 22:00; (3) the  $q_{lw}$  do not have the same shape of  $q_{lc}$ , especially close to the CT where the jump of  $q_{lw}$  drops fast with height (Figure 11 c, height 1400 m). The latter could be explained by the top more dry entrainment or by a weaker subsidence that the model could be considering.

### 3.3.2. Efficiency of the standard fog collector

The homogenization of units between fog collection and  $q_l$  described in the methodology section enables us a unification between the amount of available water in the air calculated from the parcel method and the fog collected. Figure 12.a shows the diurnal evolution of the  $q_{lc}$ ,  $q_{lw}$  and the average amount of fog collected between stations 1090 m and 1219 m. Figure 12 b shows the meteorological conditions of temperature, wind speed and relative humidity for this specific day analyzed.

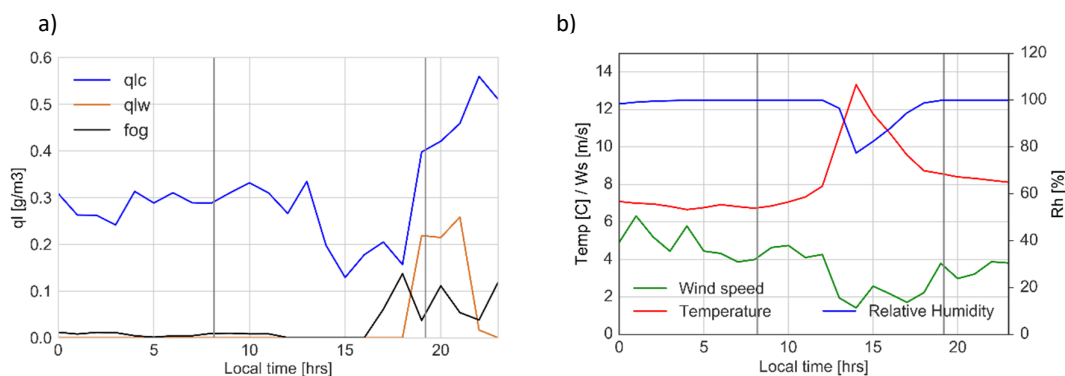


Figure 12. (a)  $q_{lc}$  corrected from the parcel method,  $q_{lw}$  simulated by WRF and fog collection distribution as a function of local time. (b) the meteorological conditions of air temperature, relative humidity (RH) and wind speed. Day analyzed 21-07-2015.

We find that the daily distribution of  $q_{lc}$  is almost constant during the night-morning (until 10:00) with values around  $0.3 \text{ g kg}^{-1}$ . It slightly decreases in the afternoon (15:00 local time) and increases again in the evening (from 18:00 local time). With similar distribution over time, the fog collection increases from early afternoon to the night (15:00). This similar behavior after 15:00 suggests that the fog collected is related to the  $q_{lc}$  and therefore can be related to the Marine Sc conditions. Regarding  $q_{lw}$ , we only found water available in the evening, with lower values around  $0.2 \text{ g kg}^{-1}$ . This can be explained by the fact that Sc clouds are only produced during the evening at the same altitudes where fog has been observed (Chapter 4, regional modeling). Also, for this reason, the water collected surpasses the available water simulated by WRF at 18:00 and 22:00.

By relating the results of the liquid water to the meteorological conditions, we are able to establish minimum threshold values for meteorological conditions, which are indicative of fog formation. Such

thresholds are between 7° to 9° C, 90% of RH, moderate wind speed in the range of 2 - 5 m s<sup>-1</sup> and cloud water content higher than 0.25 g m<sup>-3</sup>. Here, we assume that fog dissipates because it is not collected and it occurs when the meteorological values are below these thresholds. For example, during the night and early morning (before 11:00 local time) temperature, RH, and q<sub>lc</sub> conditions favor the fog collection. However, the liquid fog quantity is rather small around 0.02 g m<sup>-3</sup>. In our opinion, the wind plays a key role explaining these lower values, as wind speeds higher than 4 m s<sup>-1</sup> can negatively affect the fog collection. During field work, we have observed that droplets retained by the mesh were removed under strong winds and could not be properly collected.

In the afternoon interval between 11:00 to 16:00 local time, the increase in temperature leads to a decrease in RH resulting in fog dissipation. From 16:00 onwards, a decrease in temperature together with an increase in RH and q<sub>lc</sub> produces the highest fog collection observed during the day. If we link these meteorological conditions with the well-mixed condition of the ABL described in the previous section, we can associate this high fog values to the arrival of well-mixed Sc cloud conditions that are characteristic of the advection of oceanic air masses.

However, the lack of wind direction observations for the stations 1090 m and 1219 m, does not allow us to incorporated into the analysis. In our opinion, wind direction could play a very important role in the fog collection due to the Sc cloud entrance. The latter will be approached in the next section by the modeling results. However, observations of wind direction from the station 40 m, show as a predominant wind from SW (ocean) as observation reported in the literature as well (Cereceda et al. 2008a).

From this qualitative analysis, we find a correlation between the fog collection and q<sub>lc</sub> and a certain dependence of the wind speed and q<sub>lc</sub>, which represent the most relevant factors on the diurnal dynamics. It is important to emphasize that the wind speed is the scaling factor we used to transform the area of the mesh into the volume (Methodology section), so its influence is also key in the calculations and assumptions.

Table 2. Results of the Spearman's correlation coefficient between meteorological variables involve in fog collection.

Variable	Coefficient	P value	Significance
Cloud water content (q <sub>l</sub> )	0.15	> 0.05	No sig.
Wind speed (ws)	<b>-0.62</b>	<b>&lt; 0.005</b>	<b>Sig.</b>
Temperature (T)	<b>0.72</b>	<b>&lt; 0.0001</b>	<b>Sig.</b>
Relative humidity (RH)	-0.26	> 0.05	No sig.

To identify which meteorological variables are correlated with the fog collection, we calculated a correlation coefficient using the nonparametric Spearman's rank test (Table 2). We found that wind speed and temperature are strongly correlated with fog collection (Table 2). Wind speed is negatively correlated to fog collection as high-speed winds remove away the water droplets attached to the collector and low-speed winds favors fog collection. This can be noticeable at morning (until 11:00 local time), where values of q<sub>lc</sub> around 0.3 g m<sup>-3</sup> produce insignificant values of fog collection. This occurs even though the meteorological conditions as temperature and RH favor them (Figure 12). In Table 2, we find that temperature is positively correlated with fog collection, especially during the afternoon (from 18:00), because it influences the RH and q<sub>lc</sub>. Here basically increases in temperature above the threshold range, enhance the fog collection.

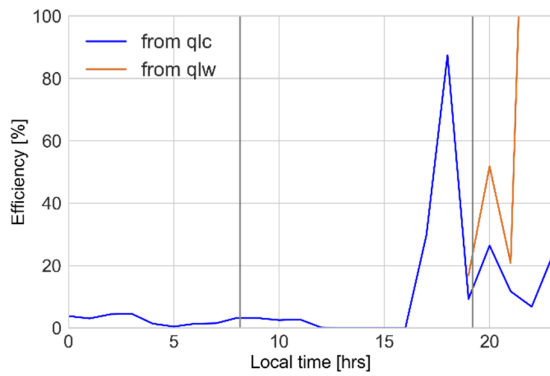


Figure 13. Efficiencies of the fog collector for  $q_{lc}$  and  $q_{lw}$ , as a function of local time. Analyzed day 21-07-2015.

This section finishes with a brief discussion on the efficiency of the fog collectors. By analyzing and calculating the ratio  $q_{lc}/\text{fog}$  and  $q_{lw}/\text{fog}$ , we estimated a first-order approximated efficiency for the standard fog collectors. Figure 13 shows the efficiency of the collectors as a function of local time for the day analyzed.

Analyzing the efficiency calculated from the inferred values of  $q_{lc}$ , we found a daily efficiency of 11.3% with peaks of 87% at 18:00 local time. This means the collectors are only able to collect around 10% of the total amount of water available in the air. If we select the moment with the highest fog

production (15:00 – 23:00 local time), the efficiency grows to 30%. The difference between fog collected and  $q_{lc}$  are largely dependent on the conversion from  $\text{m}^2$  of mesh to  $\text{m}^3$ , but also due to meteorological conditions such as temperature and wind speed and direction. The efficiency calculated from  $q_{lw}$  derived from WRF is higher than efficiency calculated from  $q_{lc}$  because its values are lower than  $q_{lc}$ . However, this efficiency is only available during the evening. In figure 13, the peak larger than 100% we find is because the fog collected exceeded the available water simulated. If we omit this peak, the daily efficiency becomes similar to the one calculated with the parcel method, i.e. 30%. To summarize, efficiency values of the fog collectors seems to be realistic regarding our field observations. In the discussion (Chapter 5) we will discuss the improvements of fog collectors in order to increase its efficiency.

#### 4. REGIONAL MODELING OF A REPRESENTATIVE FOG EVENT

This chapter contains the results and discussion concerning the modeling performed by WRF. Since in the previous sections, we have focused on the representative well-mixed day 21-07-2015, we select the same day to connect with our previous findings and provide a regional perspective of the fog in its temporal and spatial characteristics. Here, we present a vertical and horizontal characterization of the marine Sc cloud and its influence in the land, connected with our previous findings. The role of the geographical local factors is explained as well. In particular, how topography and sea surface temperature (SST) affect the development of Sc cloud over the ocean but also how it influences on the land fog system. Finally, this chapter aims to answer the third research question about if the main characteristic of the fog can be modeled at the regional level.

##### 4.1. Simulation of the Sc cloud influencing the land.

Figure 14 shows the synoptic conditions during the analyzed day 21-07-2015. These are shown to contextualize spatially the Sc cloud arrival to the continent. In terms of sea level surface pressure, we find during the all diurnal cycle low pressure above the land. In comparing values, we find a difference of 5 hPa between sea and land. The synoptic indicates that there is predominant wind from the W-SW to the research area during the whole day. At 15:00 the increases in temperature over the land make pressure decrease in 1 hPa. As a result, wind penetrated further into the continent (around 50 km). During the night (22:00 local time), the pressure is almost equal over the land and over the sea, due to the decreases in temperature (below 13° C) which results in stabilization of the winds. Due to the steep slope present in the coastal topography and its altitude, there is always a strong gradient of temperature between the land and the sea in the order of 5° C. Likewise, the topography does not allow to form a land breeze circulation, due to the changes in pressure between land and sea does not change notably. The latter is related to transport of the Sc cloud from the ocean into the land, through the main wind direction (W-SW), which is also reported by Cereceda et al, (2008b).

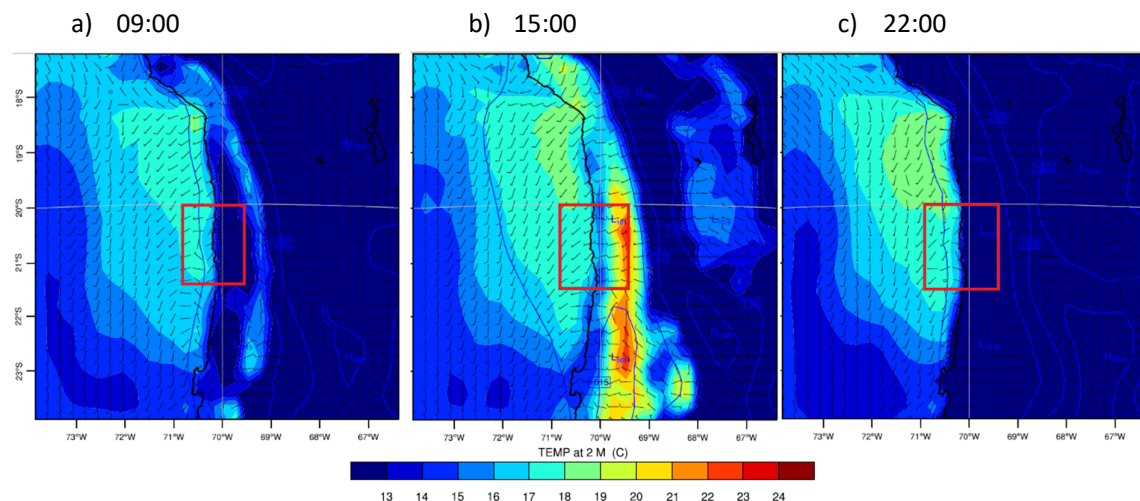


Figure 14. Synoptic conditions at 09:00, 15:00 and 22:00 local time for 21-05-2015. 2 m surface temperature ( $^{\circ}$  C) (full color), sea level pressure (hPa) (contours), wind speed (kts), and wind direction (arrows), are shown. The research area including the station site is represented by a red square.

##### 4.1.1. Vertical characterization

Figure 15 shows a cross-section of the cloud water content obtained by WRF modeling (qlw) and wind bars for the first 2000 m at 21° S, 70.8° - 69.6° W. In the cross-section the observation stations are placed on the topography, where 40 m correspond to blue, 1090 m red and 1219 m black, respectively.

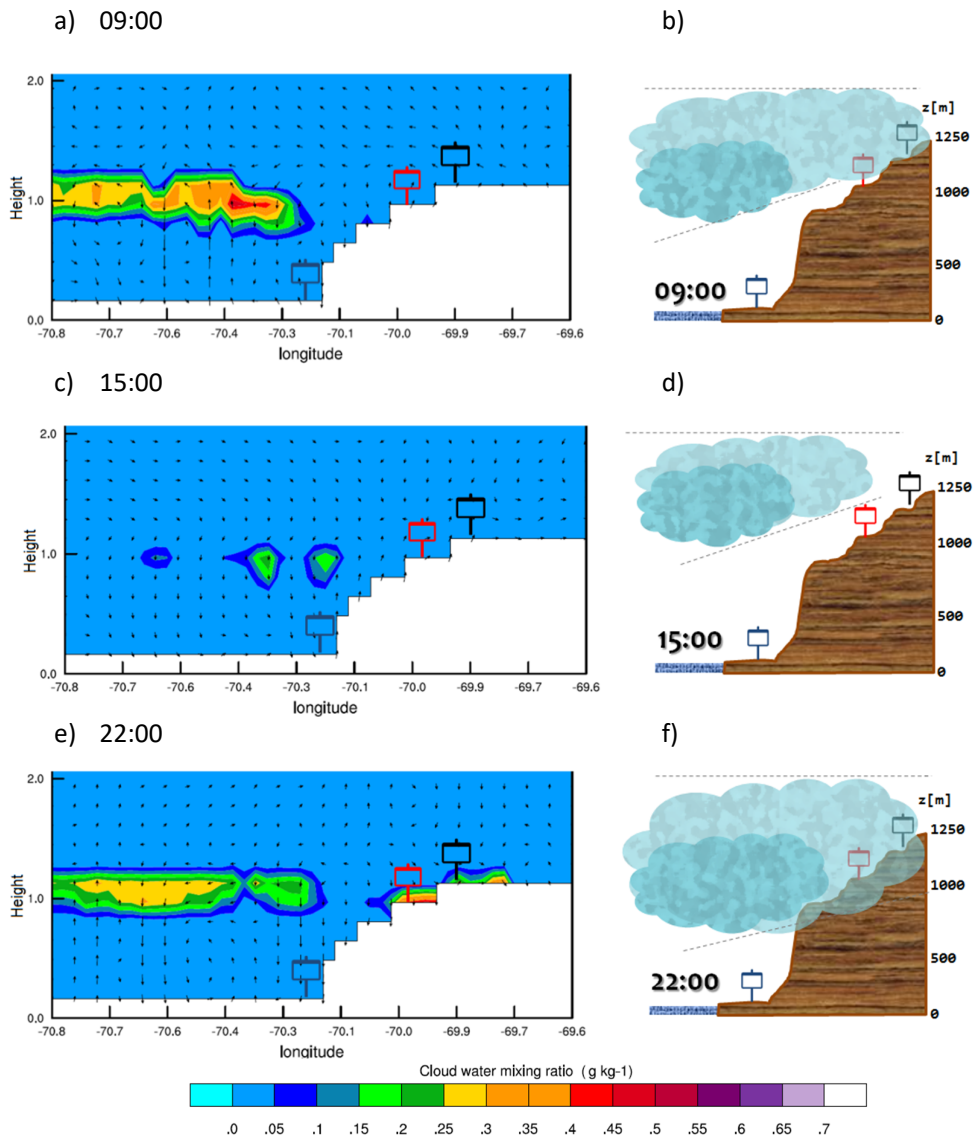


Figure 105. a, c, e: Vertical cross-section at 21°S of cloud water content (g kg<sup>-1</sup>). Arrows represent wind direction. Surface observations are placed in the topography; 40m, 1090 m and 1219 m in blue, red and black, respectively. Figure 15 b, d, f: representative schemes of cloud characteristic inferred through the parcel method (Figure 10).

Here we find a cloud layer formed at 09:00 in the ocean. This Sc cloud is present from 800 m with a CD of 160 m. The cloud deck penetrates a bit in the land. In fact, over the station, 40 m (blue) cloud is also present. The model shows that at stations 1090 m and 1219 m clouds are not present and winds blow from the land to the sea over the clouds (1.3 km). The values of CB inferred by the parcel method shows a cloud thicker than cloud modeled by WRF (Figure 15 b) and fog is observed at 1219 m (Figure 10). The model simulates a cloud that agrees with inferred values in terms of CB, but fog and cloud layer are underestimated at morning (09:00 local time). At the afternoon (15:00 local time), modeled clouds are formed over the station 40 m. However, the clouds are not yet present at 1090 m and 1219 m. In connecting this finding with the one reported in Figure 10, we find that the inferred observations report that CB reaches the CT at 1219 m. In other words, there are not clouds formed there. Regarding the latter, the simulation also does not show cloud formed at 1219 m, then it agrees with the inferred values (Figure 15 d). Finally, at night (22:00 local time) a cloud deck is reproduced over the 40 m station in the simulation. These results agree with the fog observations at 1090 m and at 1219 m).

By Analyzing the cloud water content produced by WRF (qlw) for the same three period, we find values in the same range than inferred observations and the one presented in previous observations of Sc deck (Duynerke et al. 1995) around  $0.35 \text{ g kg}^{-1}$  in the middle of the Sc cloud (Figure 11 a). During the night, at 22:00 local time, the model yield ql values that ranged from qlw 0.3 to  $0.45 \text{ g kg}^{-1}$  (Figure 15 e). Here, observations of fog show values of  $0.4 \text{ g m}^{-3}$  in average for 1090 m and 1219 m while model results calculated values of  $0.5 \text{ g m}^{-3}$  (Figure 15 f and Figure 11 a).

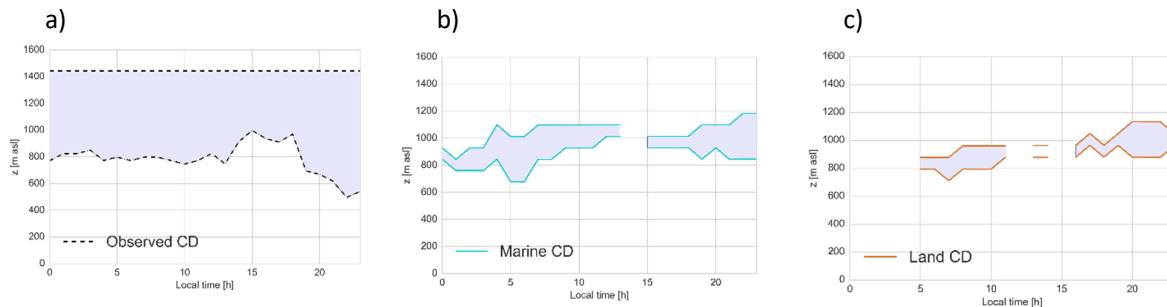


Figure 116. Cloud depth (CD) as a function of local time for; (a) inferred through surface observations, (b) modeled from a marine grid point and (c) modeled from a land grid point.

To complete the analysis, we compare the cloud layer modeled by WRF with the cloud layer inferred from surface observations and reported in the literature. Figure 16 shows the cloud layer inferred by observations compared with two WRF grid points: one over marine ( $20.5^{\circ}\text{S} - 70.8^{\circ}\text{W}$ ) and the other over land ( $20.5^{\circ}\text{S} - 70.1^{\circ}\text{W}$ ).

Table 3. Root means square error (RMSE) of cloud base (CB) and cloud top (CT) of marine grid point and land grid point, respect to the inferred CB-CT from surface observations. The standard deviation is also shown.

Grid point / s. Observations	Root mean square error [m]	Standard deviation [m]
Marine CB	162	88
Marine CT	326	82
Land CB	187	70
Land CT	305	84
S. Observation CB	-	118
S. Observation CT	-	0

First, we find some similarities between CB modeled and the one inferred from surface observations. Table 3 shows the root mean square error (RMSE) of marine and land grid point of CB and CT respect to the inferred surface observations. Here find that WRF represents better the CB than CT when we compared CB-CT. The larger RMSE presented by the CT is also related with how CT is inferred from remote sensing observations, where probably the remote sensing method performed was not accurate enough.

Second, the modeled values of cloud layer disagree with values of Sc cloud base and top reported in the literature by Duynerke et al (1995) and Garreaud and Muñoz (2004). Here, the authors report a cloud layer 300 - 500 m lower than our modeling results. These differences can be also related to the latitude, because observations in the literature have been taken around  $30^{\circ}\text{N}$ , where subsidence is higher than at  $21^{\circ}\text{S}$  where our research are is located. Likewise, as the Figure 14 e-f show, the simulation also matches with the fog observations, then could be a sort of lifting of Sc cloud when it arrives at the land.

Finally, we discuss how the cloud characteristics might vary when arriving over the land. Figure 16 b shows us the CD at a marine grid point, which is higher than above the land grid point, with average

values of 187 m and 133 m, respectively. This result indicates that the cloud layer thins when it arrives at the land, which can be related with higher sensible/latent heat surface fluxes produced by the land. Moreover, because of the thinning, the qlw tends to increase more when it is over the land than over the sea. This is proven in Figure 14 a where values of qlw over ocean and land are  $0.25 \text{ g kg}^{-1}$  and  $0.5 \text{ g kg}^{-1}$ , respectively. Another relevant process in Figure 16 c is related to the uplifting of the cloud over the land, where the CT moves from 09:00 to 22:00 local time from 876 m to 1200 m, respectively.

#### 4.1.2. Spatial variability of the fog event

Figure 17 shows spatial results of the fog spatial distribution. More specifically we show the liquid water path (LWP) in  $\text{kg m}^{-2}$  of the first 100 m from the ground. The select area corresponds to the inner domain solved with a resolution of  $1 \text{ km}^2$ . The LWP is the integration of the qlw in a certain column of air (here the first 100 m), it can be understood as the liquid water amount present in the fog.

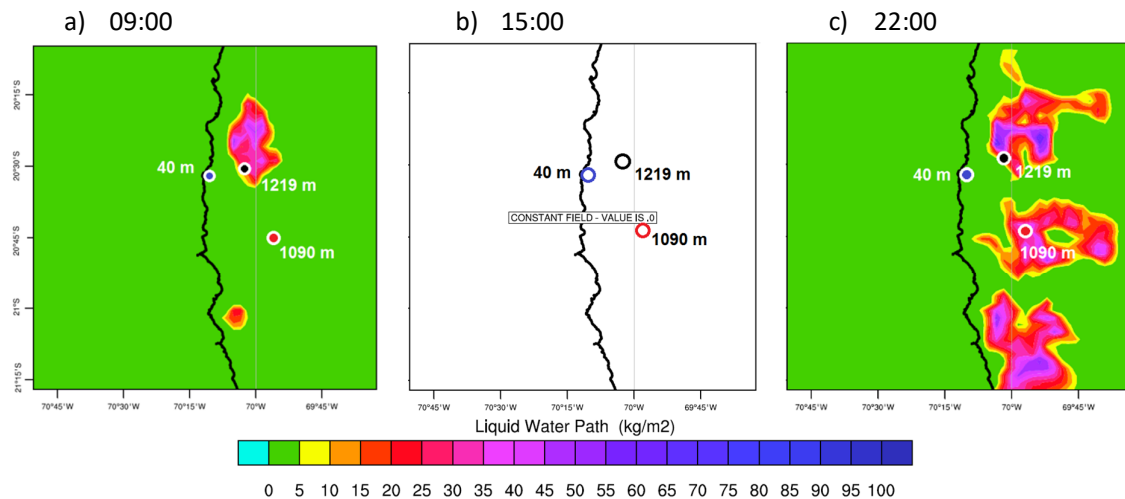


Figure 17. Liquid water path (LWP) in  $\text{kg m}^{-2}$  for the research area at 09:00, 15:00 and 22:00 local time. Surface observations are placed on the map.

This regional distribution shows fog formed at 1219 m at 09:00 local time with average values of  $15 \text{ kg m}^{-2}$ . At the same time and level, Figure 18 shows that fog observations accumulate  $0.5 \text{ l m}^{-2}$ . Here it is relevant to notice that, both model results and fog observations, indicate the absence of fog at 1090 m. During the afternoon at 15:00 local time, no fog is observed at any levels nor fog is modeled by WRF. Even though probably the Sc cloud is formed above 1090 m, this probably never touch the ground at any levels. Finally, at 22:00 local time during the night, around  $0.3 \text{ l m}^{-2}$  and  $1 \text{ l m}^{-2}$  were observed at 1090 m and 1219 m respectively (Figure 18). At the same time, the simulation in WRF shows fog formed at 1090 m and 1219 m with values around 30 and  $25 \text{ kg m}^{-2}$ , respectively. The values of LWP modeled by WRF correspond in the same magnitude to the of fog collected observations, even though the units are not comparable each other.

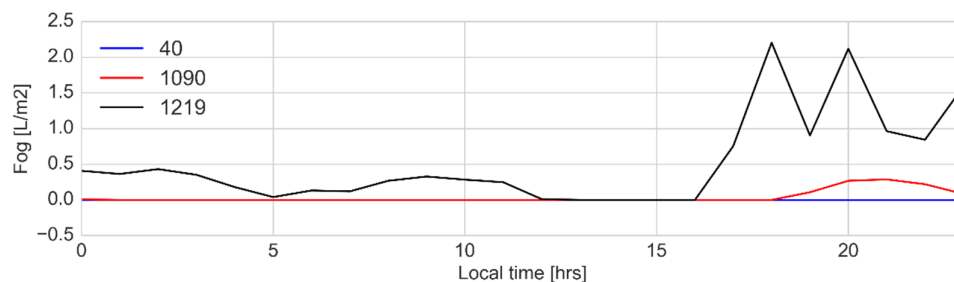


Figure 18. Fog collection observation as a function of local time at 21-07-2015, for the stations 40 m, 1090 m, and 1219 m.

In concluding, we find that WRF is able to reproduce the main characteristics of the Marine Sc with better accuracy in the prediction of cloud base than of cloud top. However, due to the simplicity in retrieving cloud top, the performance of WRF cannot be assessed properly. In terms of cloud water content, WRF simulates realistic values, which are supported by inferred observation and literature (Duynerke et al. 1995, Stevens et al. 2003). Finally, even though Sc cloud is not perfectly modeled, its influence on land understood as fog can be modeled properly. In the next section, we analyze two extra experiment to provide a first impression of the role of the geographical local factors on land fog dynamics.

#### 4.2. Importance of geographical local factors on fog dynamic

The following experiments aim to understand the importance of local geographical characteristics that involved in the fog system. Next section describes the results of two numerical experiments; a modeling in absence of topography and a modeling including changes in sea surface temperature (SST). For both experiments, the numerical experiment of marine Sc cloud and the land fog system described in the previous section is used as a control case.

##### 4.2.1. Influence of topography

Maintaining the same conditions as in the control case, we perform a new numerical experiment by modifying topography. In particular, we assume a topography flat when it is higher than 40 m. The next section describes a horizontal and vertical comparison between the modeling in absence of topography and the control case.

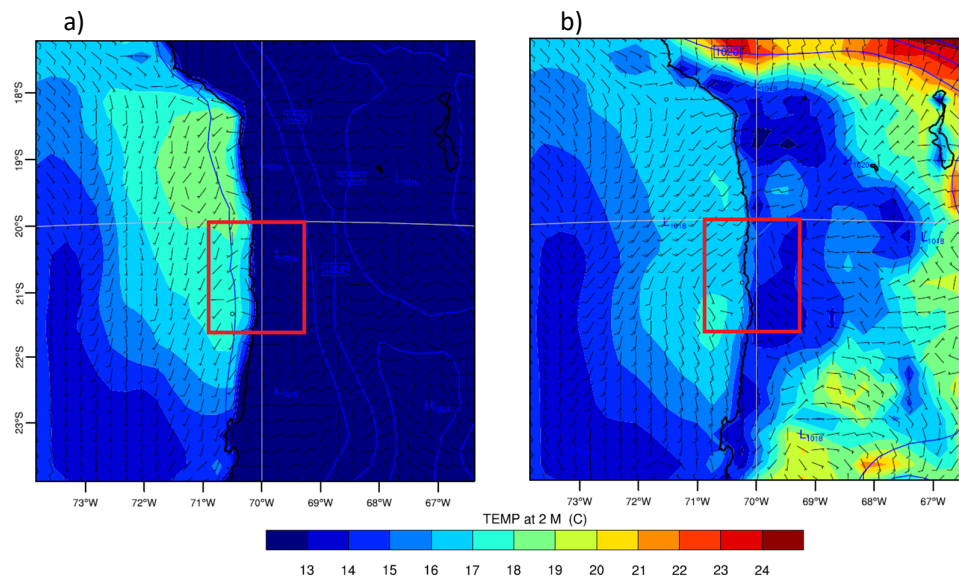


Figure 19. Synoptic conditions at 22:00 local time for (a) the control case, and (b) the modeling in absence of topography. 2 m surface temperature (full color ( $^{\circ}$ C), pressure (contours) (hPa), wind speed (kts), and wind direction (arrows) are shown. Research area is represented by a red square

Figure 19 a shows the wind circulations for the control case. We find clear differences in surface temperature between the land and the ocean. We notice the interactions between the land and the ocean are reduced to a narrow area next to the offshore (10 km), where temperature shows a strong horizontal gradient ( $7^{\circ}$ C). Contrary, the wind circulation in the experiment without topography shows so plentifully different circulation patterns. Figure 19 b shows a strong sea breeze, which cools the land farther into the continent from W toward E. From the figure, we find that topography is not only affecting the Sc cloud as a barrier, but also the structure of the atmospheric boundary layer (Figure 20). Here the boundary layer height is shallower and better mixed in absence of topography than in the

control case, probably due to the strong wind circulation of the sea breeze (Figure 21). In that respect, the steep topography induces a lift on the ABL reaching higher altitudes (1200 m) in the control case than in the topography absence case.

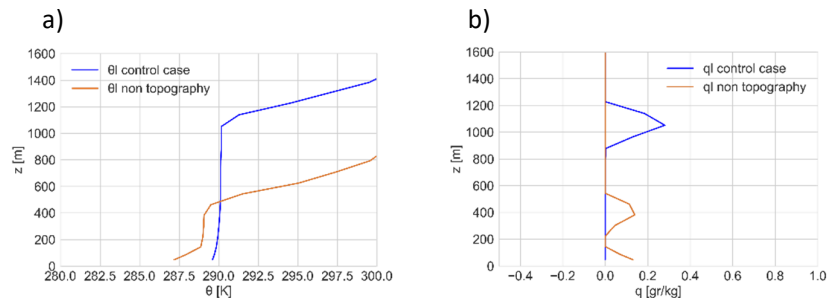


Figure 20. (a) Vertical profile of liquid water potential temperature ( $\theta$ ) for control case and simulation in absence of topography. (b) Vertical profiles of cloud water content ( $q_{lw}$ ) for control case and simulation in absence of topography. For the day 21-07-2015 at 22:00 local time.

To complete the analysis, Figure 21 shows a vertical cross-section of the cloud water content obtained by WRF modeling ( $q_{lw}$ ) for the control case and the simulation in absence of topography, at 22:00 local time. Here, we observe clearly two main components that make differences between simulations. Firstly, from the land to the sea, around 900 m there is an air flow that drops into the ocean and returns to the land at surface level (sea breeze circulation, Figure 21 b). Secondly, radiation fog is formed at land reaching almost 500 m thick and  $0.4 \text{ g kg}^{-1}$  of cloud water content at some places.

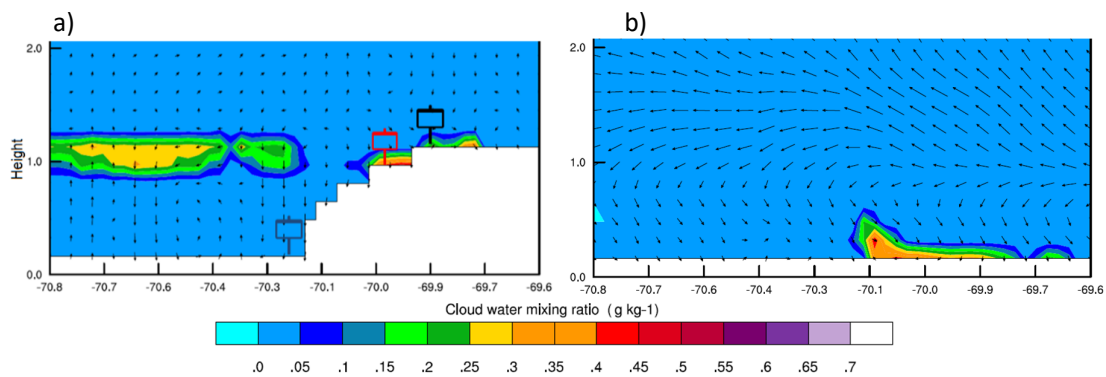
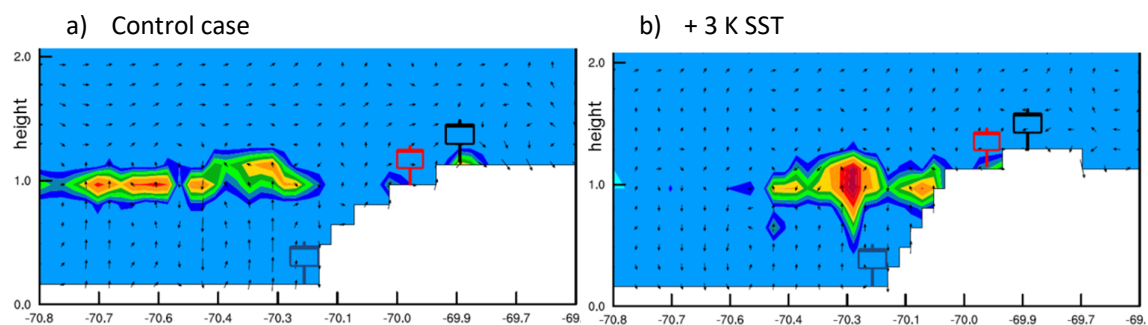


Figure 21. Vertical cross-section at  $21^\circ\text{S}$  of cloud water content ( $\text{g kg}^{-1}$ ) for (a) control case and (b) simulation in absence of topography. For the day 21-07-2015 at 22:00 local time.

#### 4.2.2. Influence of sea surface temperature

The SST is changed in order to understand the importance of this quantity in enhancing the Sc cloud and fog formation. The next section describes the results of this experiment.



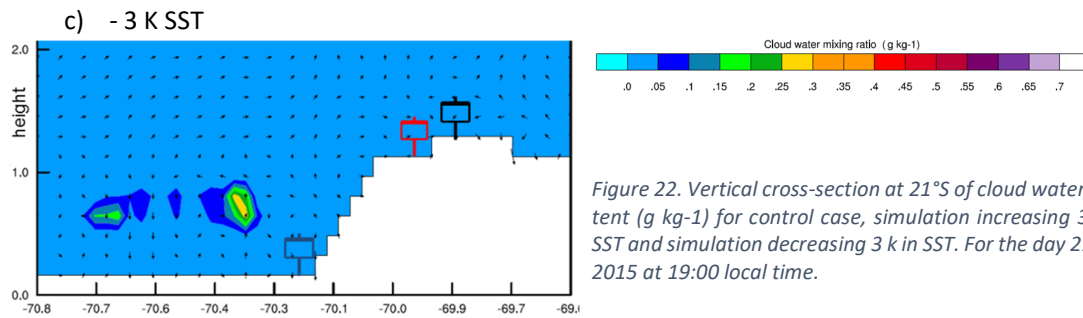


Figure 22. Vertical cross-section at 21°S of cloud water content (g kg<sup>-1</sup>) for control case, simulation increasing 3 k in SST and simulation decreasing 3 k in SST. For the day 21-07-2015 at 19:00 local time.

Figure 22 shows the cross-section of liquid water content for the control case and simulations with changes in 3K SST. The figure represents at 19:00, where the highest values of fog collected has been observed (Figure 18). Here we observe that in a warmer ocean the Sc cloud increases their thickness. We also observe that the cloud deck reaches the mountain at higher levels. In other words, the Sc cloud formed under a warmer ocean produces more fog from 800 m to 1220 m (Figure 22 b). Also, we find increases in the cloud water content from 0.3 to 0.5 g kg<sup>-1</sup> in the core of the cloud. Contrary, when SST decreases 3 K the Sc cloud forms very shallow clouds. Sc is almost not formed and their cloud water content decreases in the order of 0.25 g kg<sup>-1</sup> (Figure 22 c).

The Sc cloud formation is therefore very sensitive to the changes in SST. Increases in SST seems to increase the evaporation from the ocean producing more cloud cover, but also clouds with more water. Likewise, decreases in SST seems to decrease the evaporation fluxes from the ocean, producing less cloud cover, more dry clouds and also a shallower atmospheric boundary layer.

## 5. DISCUSSION

Our findings need to be placed in perspective. Firstly, the retrieval of cloud characteristics using surface observations can be improved in order to have more accurate descriptions and characterizations. Regarding the parcel method used to infer the cloud base (CB), our estimations are realistic validated against fog collection measurements and also with WRF modeling results. However, because no flight observations or radiosondes have been taken in the research area, the CB inferred have not been fully validated. Regarding the latter, ceilometer measurements can be used to validate or correct the CB through the parcel method. Similarly, the adiabatic cloud water content ( $q_{la}$ ) obtained from the parcel method as well, can be also improved and calculated in a more physical sounded manner. For instance, by including the mixing of the environment air during parcel ascent, we can obtain realistic results. Now, the correction factor applied to obtain more realistic values supported in observations (Methodology, Section 2.1.5), although it corrects does not consider these physical processes. Regarding the latter, the correction factor also can be improved by incorporating radiosonde measurements to correct values of  $\Theta$ ,  $q$ , and  $q_l$  in order to create a correction factor that depends on height, season and also latitude.

Similarly, and as discussed in the results, our estimation of CT is limited and without including the diurnal variability. In spite of the good agreement with typical cloud top of Sc cloud deck, potential improvements can be made in two ways. Firstly, incorporating satellite products of cloud cover fraction with high spatial and temporal resolution (GOES and METEOSAT for instance). In that way, not only the precision of the CT level can be improved, but also its diurnal variability, which for now is assumed to be constant on time. Secondly, radiosonde measurements also could set properly the CT and its diurnal variability could be improved through an accurate modeling that suits the CT of the observations.

The importance of surface observations lies not only in the availability of this information but also in the continuity in the time of this type of measurements. Although in situ observations as flight measurement campaigns, radiosondes and satellite observations can give us a very precise information about the cloud characteristics, they are not constant at the time. Here, the surface observations play a key role in the monitoring tasks, because they are very available and also constant in the time. However, the surface observations must have high quality and measure as many variables are possible, in order to avoid assumptions. Through this work, we attempt to approach to the accurate use of surface observations to characterize the marine Sc cloud. In that way, in the near future be able to use it as an input in the fog harvesting forecast and monitoring.

Another remarkable fact is the use of the combination of surface observations and the local topography. As it was shown in the results, the well-mixed and stratified regimes were defined using the surface observations placed on a steep slope facing the ocean, simulating a meteorological tower. Our findings here demonstrated the strong influence of marine boundary layer (MBL) in the first 20 kilometers inland. By taking advantage of the steep and high orography of the coast Atacama Desert, we could optimize this combination between surface observations and topography. By finding steeper and near to the coast places to install meteorological stations we could have a better understanding and monitoring of the marine Sc cloud both in vertical and also in the time dimension. The coast of the Atacama Desert has plenty places that can reach these requirements. For example, the Cerro Tolar reaches 1700 m at 5 km from the offshore, presenting perfect topography conditions to study the marine boundary layer, by using the methodology this work propose.

Our findings made an approach to the physical relation between fog collected and the cloud water content. Through some assumptions, we compared the amount of water collected from water available in the cloud and also a sort of efficiency of collectors. However, this first step can be improved by including accurate horizontal wind observations and decreasing the time interval between measurements. As it was presented, horizontal wind speed plays a key role in the fog collection. This is not only because the velocity affects its efficiency, but also because in the calculations to compare fog collected

with cloud water content, use the wind speed to transform the mesh area into a volume ( $\text{m}^2$  to  $\text{m}^3$ ). In that context, an accurate horizontal and perpendicular wind speed to the collectors could help us to improve this physical relation and therefore to have a more accurate result. A second improvement is decreasing the interval time where the observations have been taken. By installing better sensors to measure wind speed, fog collection and humidity every second, avoiding the errors that hourly averages carry up. Regarding the latter, another important issue to discuss is the fog collector design (Regalado & Ritter 2016). Our findings demonstrated that the wind speed affects negatively the fog collection. That because of winds higher than  $4 \text{ m s}^{-1}$ , remove the droplets caught in the collector. In order to measure the whole fog than collector catch and its relation with wind speed, improvements in the collector design have to be made.

Finally, for the regional modeling in WRF, improvements in terms of the parameterization schemes, initial boundary layer condition (IBLC), and vertical resolution need to be considered. Firstly, an in using the planetary boundary layer schemes to represent better the Sc cloud deck (Bretherton & Park 2009), we have found that our system is sensitive to the physical parameterizations. However, so far is still difficult to adequately calculate the Sc deck because the model simulates lower and thinner clouds. In this context, more experiments with different parameterizations must be performed to obtain a better representation of the marine Sc cloud over the land and the sensitivity to the physical parameterizations. Secondly, authors indicate that reanalysis data (IBLC) not always agree with the real condition of the southern hemisphere (Swart & Fyfe 2012), concluding that due to the lack of observations the reanalysis data are unreliable in the southern hemisphere (Son et al. 2010). Related to this, sea surface temperature corrections of  $+1.5 \text{ K}$  were made in the ECMWF data for the simulations performed in WRF. Therefore, to model a more accurate Sc cloud deck in the southern hemisphere, the selection of the best IBLC has to be considered carefully. Thirdly, improvements of the vertical resolution WRF can also be made. As we are studying a boundary layer cloud, which lies within the first 2000 m of the atmosphere, the vertical resolution of this section needs to be higher. For the modeling performed in this work, 20 vertical levels were used within the first 2000 m. Despite this, the number of vertical levels is not enough to represent in detail the Sc cloud, which depth goes around 500 m thick. A higher vertical resolution allows us as well to compare more accurately the cloud water content modeled with the obtained from fog observations. In that way, we could avoid the bias produced by the height average of ql, to match the height of fog observations.

## 6. CONCLUSION

Regarding the three main research questions posed in the introduction, we have obtained a first-order characterization of the marine stratocumulus physics and its influences on the land. We have proven that surface observations can be very valuable measurements to infer a vertical cloud characterizations.

The surface observations show us that the land fog system on the Atacama Desert and the Marine Sc cloud are formed under well-mixed atmospheric boundary layer regime. Here physical processes and geographical factors play an important role in its dynamic. Physical processes as the surface heat fluxes influence the cloud base affecting the cloud depth but also the fog formation, maintenance, and dissipation. Additionally, the subsidence produced by the Hadley cell downward flux, influence the cloud top variability. Both processes produce annual, seasonal and diurnal changes in the cloud layer. Moreover, dynamics of the cloud layer are also very related to the land fog collection. Finally, the topography plays a key role in the fog formation, working as a barrier for the clouds that go into the continent.

Regarding the fog collection, this can be related quantitatively to the cloud water content. We conclude that air temperature, wind speed, and cloud water content are the most important factors for the interpretation of the fog events. These meteorological conditions set thresholds between the fog formation, maintenance, and dissipation which can be very useful to design a fog index. The threshold ranges from 5-7 °C, 0.25 g kg<sup>-1</sup> of q<sub>lc</sub>, and between 2-4 m s<sup>-1</sup> of wind speed as a minimum value where fog is present. In terms of efficiency, our estimations indicate that fog collected represents 30% of the potential water available in the air, reaching peaks of 87% in the most productive hours (evening).

All these previous results based on surface observations can be better placed by performing mesoscale numerical experiments, by using the WRF model. Here we find that cloud base and cloud water content agree with the inferred observations, but also with marine Sc cloud observations reported in the literature. Even though the simulation of the Sc cloud is not able to reproduce the interaction of the cloud deck with the coast, our WRF surface results in the upper stations, coincides with the fog observations vertically, spatially and also in its diurnal evolution. Finally, the geographic local factors play a key role in the fog formation. We found that the topography plays a key role in the local circulation of winds. This influence is not only as a barrier of the Sc cloud deck but also influence the synoptic conditions between land and the ocean. The Marine Sc cloud formation is very sensitive to changes in sea surface temperature. Here increases in 3 K enhances the cloud formation and also its influences over the coastal mountains, but also lift the level of the cloud base. Contrarily, a decrease in 3 K in sea surface temperature leads the formation of shallower Sc clouds and also dissipates almost whole Sc cloud over the ocean.

Finally, correct modeling in WRF in terms of vertical and horizontal distribution of Sc over the land and a better relation between q<sub>l</sub> and fog collection can set the base of the forecasting of fog harvesting.

## 7. REFERENCES

- Aravena, R., 1995. Isotope Hydrology and Geochemistry of Northern Chile Groundwaters. *Bull, Ins fr. etudes andines*, 24, pp.495–503.
- Bretherton, C.S. & Park, S., 2009. A new moist turbulence parameterization in the community atmosphere model. *Journal of Climate*.
- Cereceda, P. et al., 2008a. The climate of the coast and fog zone in the Tarapacá Region, Atacama Desert, Chile. *Atmospheric Research*, 87(3), pp.301–311.
- Cereceda, P. et al., 2008b. The spatial and temporal variability of fog and its relation to fog oases in the Atacama Desert, Chile. *Atmospheric Research*, 87(3), pp.312–323.
- Duynkerke, P.G., Zhang, H.Q. & Jonker, P.J., 1995. Microphysical and Turbulent Structure of Nocturnal Stratocumulus as Observed during ASTEX. *Journal of the Atmospheric Sciences*, 52(16), pp.2763–2777.
- Garreaud, R.D. & Munoz, R., 2004. The diurnal cycle in circulation and cloudiness over the subtropical southeast Pacific: A modeling study. *Journal of Climate*.
- Judah Cohen, Karl Pfeiffer & Jennifer Francis, 2017. Winter 2015/16: A Turning Point in ENSO-Based Seasonal Forecasts. *Oceanography*, Vol. 30, No. 1, pp.82–89. Available at:
- Klemm, O. et al., 2012. Fog as a fresh-water resource: Overview and perspectives. *Ambio*.
- Muñoz, M. et al., 2001. Fog oases during the El Niño Southern Oscillation 1997-1998, in the coastal hills south of Iquique, Tarapacá Region, Chile. *Revista Chilena de Historia Natural*, 74.
- Osses, P. et al., 2005. La nube estratocumulo en Tarapacá, Chile. Validación de imágenes GOES mediante observación en tiempo real. *Revista de Geografía Norte Grande*, 33, pp.131–143.
- Oyarzún, J. & Oyarzún, R., 2011. Sustainable development threats, inter-sector conflicts and environmental policy requirements in the arid, mining rich, northern Chile territory. *Sustainable Development*, 19(4), pp.263–274.
- P. Cereceda, P. Osses, H. Larrain, M. Farías, M. Lagos, R. Pinto, R.S.S., 2002. Advective, orographic and radiation fog in the region, Chile Tarapaca. *Atmospheric Research*, 64, pp.261–271.
- Pilié, R.J. et al., 1979. The Formation of Marine Fog and the Development of Fog-Stratus Systems along the California Coast. *Journal of Applied Meteorology*, 18(10), pp.1275–1286.
- Regalado, C.M. & Ritter, A., 2016. The design of an optimal fog water collector: A theoretical analysis. *Atmospheric Research*, 178, pp.45–54.
- Schemenauer, R.S. et al., 1994. A Proposed Standard Fog Collector for Use in High-Elevation Regions. *Journal of Applied Meteorology*, 33(11), pp.1313–1322.
- Schemenauer, R.S. & Cereceda, P., 1994. Fog collection's role in water planning for developing countries. *Natural Resources Forum*, 18(2), pp.91–100.
- Schewe, J. et al., Multimodel assessment of water scarcity under climate change.
- Siebesma, A.P. et al., 2003. A Large Eddy Simulation Intercomparison Study of Shallow Cumulus

Convection. , 60(10).

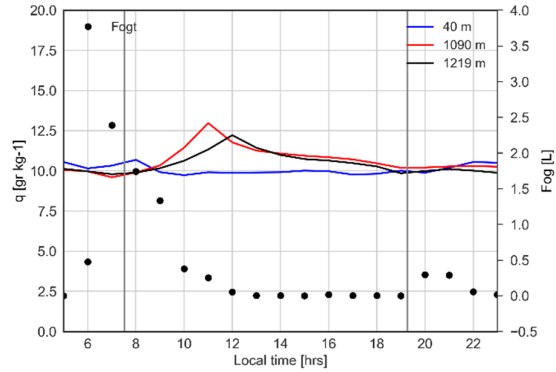
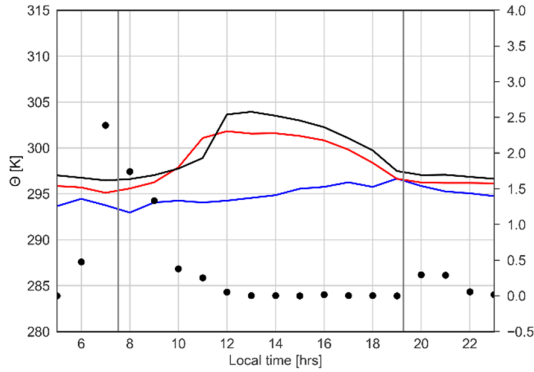
- Son, S.-W. et al., 2010. Impact of stratospheric ozone on Southern Hemisphere circulation change: A multimodel assessment. *Journal of Geophysical Research*, 115(D3), p.D00M07.
- Stevens, B. et al., 2003. Dynamics and Chemistry of Marine Stratocumulus - DYCOMS-II. *Bulletin of the American Meteorological Society*.
- Swart, N.C. & Fyfe, J.C., 2012. Observed and simulated changes in the Southern Hemisphere surface westerly wind-stress. *Geophysical Research Letters*, 39(16), pp.6–11.
- Wesichet, W., 1975. Las condiciones climáticas del desierto de Atacama como desierto extremo de la tierra. *Revista de Geografía Norte Grande*, 1, pp.3–4.
- Wyant, M.C. et al., 2010. The PreVOCA experiment: Modeling the lower troposphere in the Southeast Pacific. *Atmospheric Chemistry and Physics*.
- Zhang, C., Wang, Y. & Hamilton, K., 2011. Improved Representation of Boundary Layer Clouds over the Southeast Pacific in ARW-WRF Using a Modified Tiedtke Cumulus Parameterization Scheme \*. *Monthly Weather Review*.

8. APPENDIX

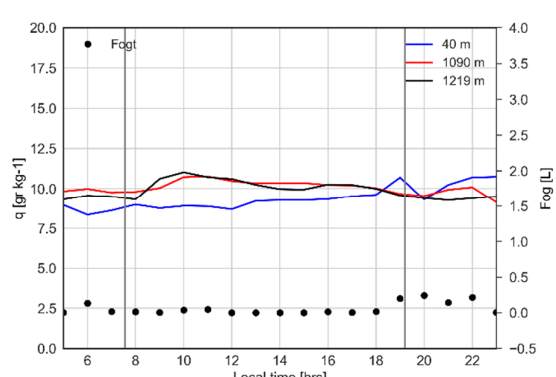
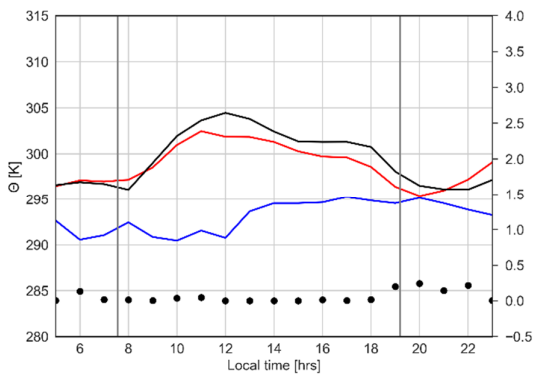
8.1. Well-mixed and stratified regimes analyzed

8.1.1. Well-mixed

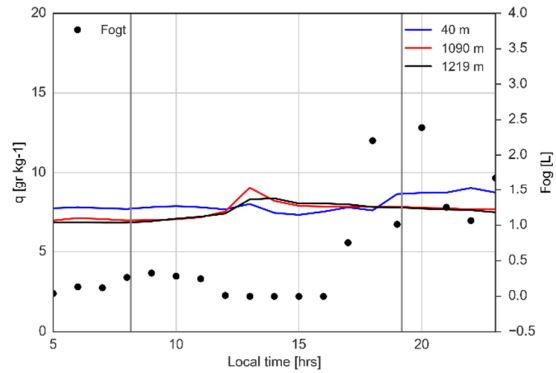
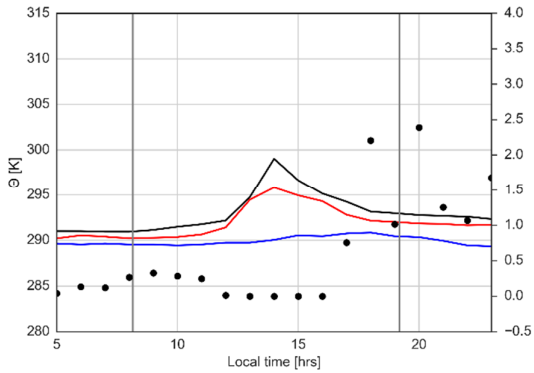
18-04-2015



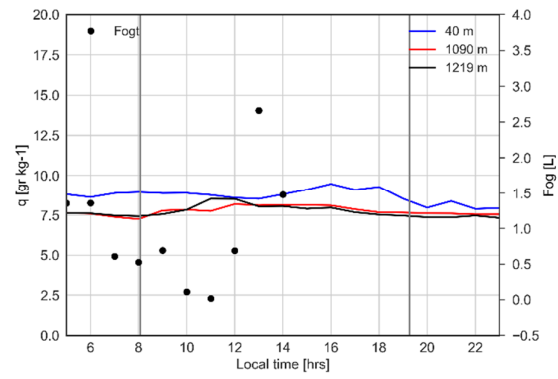
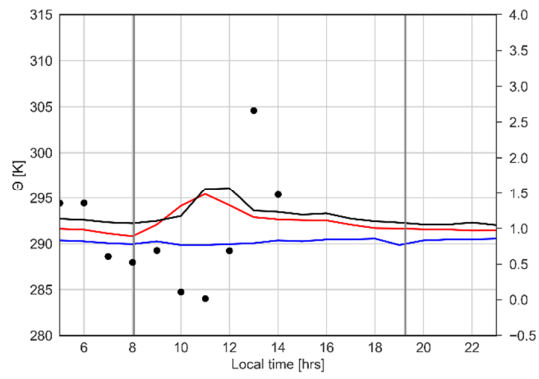
29-04-2015



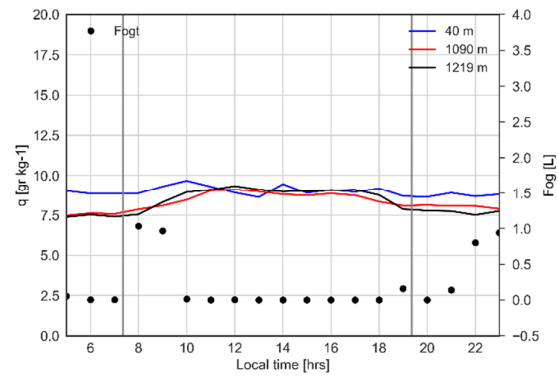
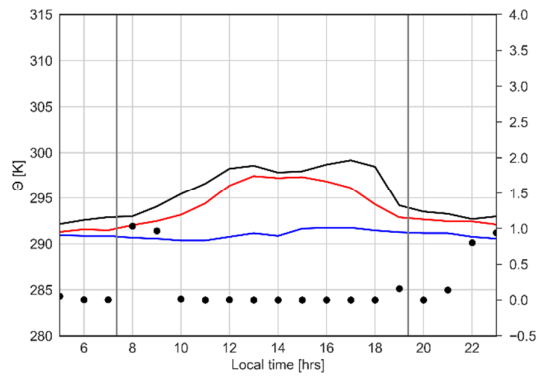
21-07-2015



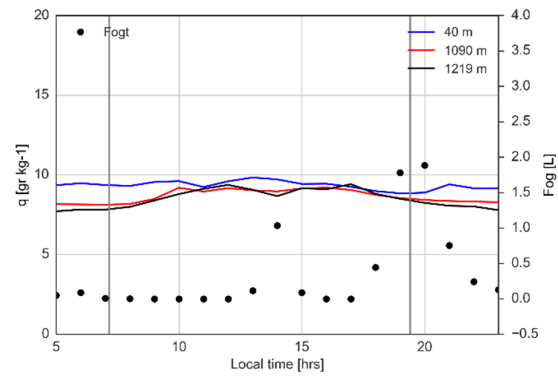
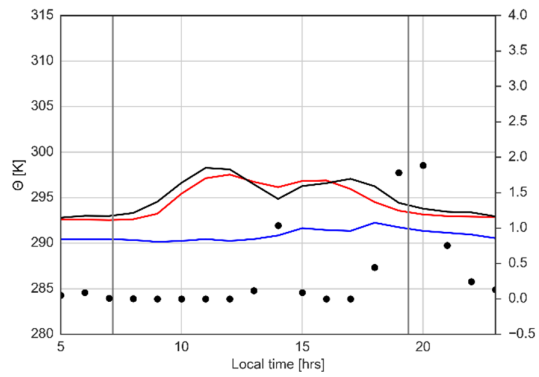
08-08-2015



17-09-2015

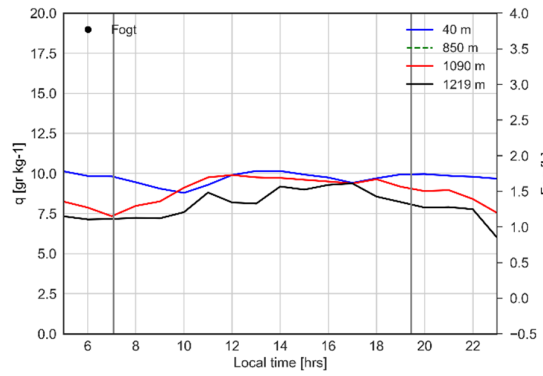
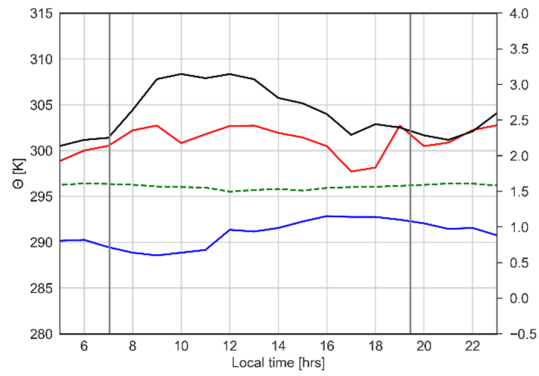


08-10-2015

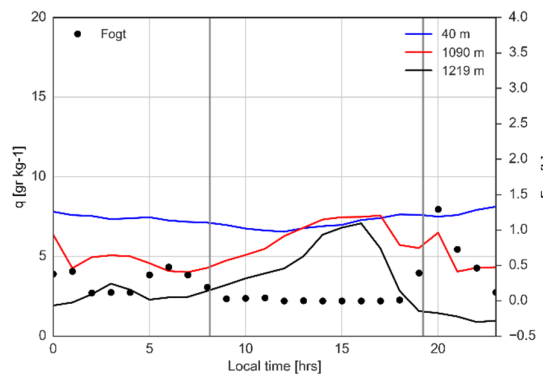
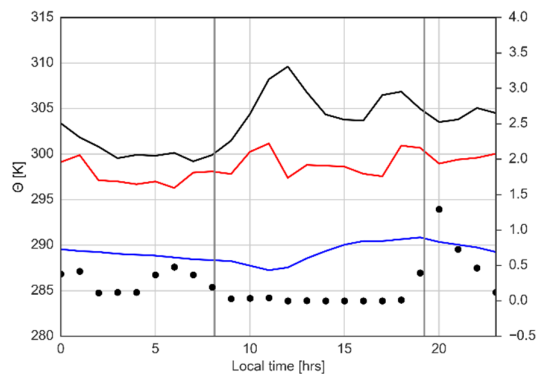


## 8.1.2. Stratified

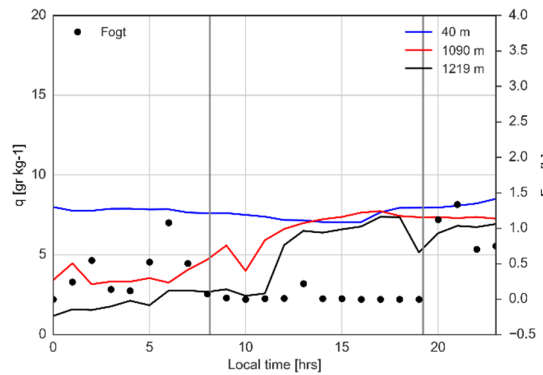
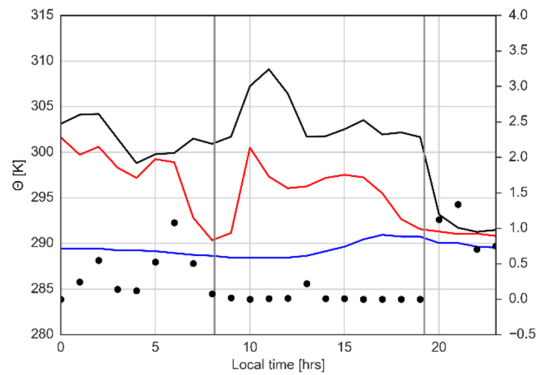
20-07-2015



27-07-2015



28-07-2015



## 8.2. Diurnal variability of the well-mixed days

